https://doi.org/10.5194/wes-2026-103
Preprint. Discussion started: 18 September 2026

Open Access
WIND ENERGY SCIENCE DISCUSSIONS

A comprehensive evaluation and uncertainty quantification of offshore turbulence intensity from WRF mesoscale simulations

Sandra Schwegmann[1], Tanguy Lunel[2,3], Lukas Vollmer[1], and Martin Dörenkämper[1]

[1]Fraunhofer IWES, Oldenburg, Germany
[2]France Energies Marines, Plouzané, France
[3]Centre National de Recherches Météorologiques, Université de Toulouse / Météo-France / CNRS, Toulouse, France

Correspondence: Sandra Schwegmann (sandra.schwegmann@uni-oldenburg.de)

Abstract. At the beginning of each wind energy project, an as accurate as possible characterization of the site-specific wind resources is needed for any economic considerations of the project. Besides wind speed and direction, which can be measured easily and of which the representation in models has been investigated in various studies, information about wind turbulence suffers from a lack of confidence yet, although it is one of the key parameters that define the lifetime of wind turbines, and its characteristics are of high importance already in the planning phase. In this study, we analyse the feasibility of the Weather Research and Forecasting Model to represent this turbulence in terms of turbulence intensity (TI) over a full year in the North Sea and quantify the range of uncertainties. The impact of the planetary boundary layer scheme used for model simulation on these uncertainties was investigated as well as the usage of model-resolved and subgrid-scale turbulence. Furthermore, results were evaluated for increasing spatial resolution in the model and stability impacts. It was found that TI values based on subgrid-scale turbulent kinetic energy (TKE) are significantly closer to observations than model-resolved TI (i.e. based on standard deviation of wind speed or wind speed components). As modelled TKE decreases with increasing resolution, the factor used in the TI calculation needs to be adapted to obtain comparable TI to observations. Nevertheless, independent of the planetary boundary layer scheme, resolution and test location in the North Sea, the lowest errors for TI are around 0.024 for the root mean square error (RMSE) and 30% for the mean absolute percentage error (MAPE). For any further improvement either LES simulations or a kind of correction method like Measure-Correlate-Predict (MCP) becomes necessary.

1 Introduction

In the wind energy industry, turbulence intensity (TI), which refers to the intensity of velocity fluctuations, is the most common metric to express turbulence (Tai et al., 2023). Knowledge of TI is of high interest as turbulence has an impact on power generation and wind turbine fatigue load (Tai et al., 2023; Ren et al., 2018; Yang et al., 2017; Wharton and Lundquist, 2012a) and thus for turbine class selection (Larsén et al., 2025). While wind speed and direction measurements are well established and its representation in models has been investigated in various studies (e.g. Hahmann et al., 2020; Dörenkämper et al., 2020; Saadatabadi et al., 2024), information about wind turbulence suffers from a lack of confidence yet. This has consequences for the accuracy of all second-order variables depending on TI. One of these second-order variables is the prediction of power output and consequently the annual energy production of wind turbines. It turned out that power output predictions may vary

https://doi.org/10.5194/wes-2026-103
Preprint. Discussion started: 18 September 2026

significantly even when the 10-minute averaged wind speeds are identical. The variability in atmospheric stability and thus turbulence, which is not necessarily reflected in the mean wind speed, are potential drivers for these differences (Clifton and Wagner, 2014; Wharton and Lundquist, 2012b; Dörenkämper et al., 2014). It has been shown that power output may be underestimated mostly at rated wind speeds and during convective periods while it may be overestimated at moderate wind speeds and during stable conditions (e.g. Sheinman and Rosen, 1992; Rosen and Sheinman, 1994; Kaiser et al., 2007; Albers et al., 2007; Wharton and Lundquist, 2012a; Bardal and Sætran, 2017). Lundquist and Clifton (2012), Wharton and Lundquist (2012b), and Dörenkämper et al. (2014) quantified power production variability to reach 15% to 20% between periods of high and low TI. These findings indicate that a more accurate representation of the spatio-temporal variability of TI may lead to improvements in power production predictions (Tai et al., 2023).

With the goal to increase offshore wind energy world wide there is a relevant need in reliable TI predictions. Offshore atmospheric conditions may generally be less turbulent compared to onshore conditions, due to the comparable smooth sea surface which forces less shear-generated turbulence (Bodini et al., 2020). Nevertheless, convective systems and storms lead to phases with high turbulence also offshore, but due to the remoteness and harsh environment, less measurements are available for the quantification of spatial-temporal turbulence (Tai et al., 2023). To overcome this lack of information numerical weather prediction and - more recently - also large-eddy simulations (LES) have been used to simulate the spatio-temporal turbulence in offshore regions. The Weather Research and Forecasting (WRF) model (Skamarock et al., 2019) is one of these very common atmospheric models used in wind energy science to simulate wind characteristics on mesoscales (Hahmann et al., 2020; Dörenkämper et al., 2020, e.g.).

Due to the resolution in the order of a couple of kilometers, mesoscale models cannot explicitly resolve the atmospheric turbulence processes (Larsén et al., 2025), as those occur in the order of tens of meters or lower (Peña and Mirocha, 2024). The effect of turbulence on the larger-scale flow is rather parameterized as subgrid-scale (SGS) process within the planetary boundary layer (PBL) schemes (Peña and Mirocha, 2024). There are a couple of PBL schemes available for WRF. Schemes considering the local mixing, i.e. turbulence exchange between adjacent grid cells, provide SGS turbulent kinetic energy (TKE) as output variable, which is one of the parameters that can be used for TI calculations. However, as the turbulence is parameterized, it might not fully represent the turbulence characteristics as LES simulations could, which - when properly done - resolve the dominating turbulence directly and only a small fraction is contributing on the sub-scale.

The mesoscale model WRF can also be run in LES mode with spatial resolutions of up to a couple of meters. Some studies regarding WRF TI performance based on WRF-LES calculations exist (e.g. Peña and Santos, 2021; Peña and Mirocha, 2024; Kilroy et al., 2024). However, LES simulations are computationally expensive (Tai et al., 2023) and can - even with large computational power - often only be done for very limited areas and short periods (e.g. Larsén et al., 2025; Rohrig et al., 2019) spanning over a couple of days to a few months.

Over such short periods, the seasonal and inter-annual variability of the turbulence cannot be captured, which are nevertheless relevant for several site assessment tasks. Thus, mesoscale models may become a reasonable compromise between accuracy and feasibility in terms of computational costs and resources as soon as we understand the capabilities of different model setups to represent the variability and thus the turbulent kinetic energy.

https://doi.org/10.5194/wes-2026-103
Preprint. Discussion started: 18 September 2026

Tai et al. (2023) validated TI from WRF simulations with 2 km resolution with the MYNN (Nakanishi and Niino, 2009) PBL scheme against lidar based TI for a couple of months in 2020 for the U.S. north-east coast using both SGS and wind fluctuation based calculations. They found that while wind speeds from the model well align with observations, TI is usually underestimated. In this study, we want to evaluate as to whether these findings are also valid for the North Sea and extend the analysis by considering a full year. Within this frame, we also investigated the impact of different seasons. Furthermore, we added an evaluation of the impact of atmospheric stability and varying spatial resolutions.

Several studies investigated the impact of PBL schemes on different meteorological parameters like temperature, moisture and wind speed beyond others (e.g. Banks et al., 2016; Yu et al., 2022; Yang et al., 2013; Floors et al., 2013; Deppe et al., 2013; Sathyanadh et al., 2017; Hahmann et al., 2020). Results vary between these studies and no particular PBL scheme could be identified to be the overall appropriate one. The choice rather depends on site specific conditions induced by the location as well as the considered year and atmospheric stability. These circumstances show clearly that validation and evaluation is needed for each new area and study case. To our knowledge, no study exists yet which evaluated the sensitivity of turbulence intensity to WRFs PBL schemes in heights close to common turbine hub heights of modern wind turbines above the North Sea. Therefore, we also investigated which PBL scheme out of four selected ones is best suitable for the representation of turbulence in WRF for the region of interest.

WRF cannot provide TI directly, it rather needs to be derived from other turbulent quantities. In literature, there are various suggestions how to calculate TI from different combinations of wind components and their standard deviations - hereafter referred to model-resolved TI - as well as from modelled TKE (e.g. Tai et al., 2023; Siddiqui et al., 2015; Larsén, 2022) - hereafter referred to SGS TI. Hence, our main objective is to identify an optimal combination of WRF PBL parameterization and TI calculation method and to evaluate and quantify the representativeness of TI from commonly used WRF mesoscale simulations for the North Sea over a full year.

In Section 2 we describe the data and calculation methods we used. Section 3 shows the impact of the PBL scheme and calculation method (3.1), spatial resolution (3.2) and atmospheric stability (3.3) on results. Furthermore we address the challenge in evaluating model results against different measurement devices as well as the reproducibility of results for a different location (3.4) and a different mesoscale model (3.5).

2 Data and methods

For this study we performed mesoscale simulations over a full year around two locations providing measurements for validation: IJmuiden and FINO-3. At both stations, wind measurements from meteorological masts (met masts) are available. On top, at IJmuiden also vertical profiling lidar measurements are available which helps to identify biases caused by different measurement principles. This section provides an overview of the models and observations used and lists the equations applied for the TI calculations.

https://doi.org/10.5194/wes-2026-103
Preprint. Discussion started: 18 September 2026

2.1 Model data

The two mesoscale models used in this study are WRF and the Application of Research to Operations at MEsoscale (AROME) model. WRF serves as the main model for our analysis while using the AROME model intends to verify findings from the WRF simulations.

2.1.1 WRF

For the two sites investigated in this study, WRF, which has been well-established in wind energy applications for several years (e.g. Hahmann et al., 2020; Dörenkämper et al., 2020; Fischereit et al., 2022; Gottschall and Dörenkämper, 2021) has been used in its version 4.5 (Skamarock et al., 2019). The simulations were performed using three nested domains with horizontal grid spacing of 18 km (outermost domain), 6 km (middle domain) and 2 km (innermost domain), which have been centered at the individual met mast locations. For sensitivity studies over varying spatial resolutions, simulations with an outer domain grid spacing of 27 km and inner domain resolutions of 3 km, 1 km, 333 m and 111 m (D03, D04, D05 und D06) were additionally performed. Figure 1 shows the domain boundaries on top of a regional map with the averaged wind speed in 2013 extracted from the New European Wind Atlas (NEWA) (Hahmann et al., 2020; Dörenkämper et al., 2020).

Table 1. Overview of performed simulations regarding used PBL scheme, spatial resolutions and TKE availability.

PBL scheme	3DTKE	MYNN	SH	YSU
k output	x	x	x	-
18/6/2 km	x	x	x	x
27/9/3/1/0.3/0.1 km	x	-	x	-

The model setup used here is based on best practice experience found for mesoscale models in wind energy applications (e.g. Dörenkämper et al., 2015; Gottschall et al., 2018; Hahmann et al., 2020). Thus, the set of physical parameterizations applied in this study consists of the Noah land surface model (Tewari et al., 2004), the Single-Moment (WSM) 5-class scheme (Hong et al., 2004) to account for microphysical processes, the Rapid Radiative Transfer Model for GCMs (RRTMG) shortwave and long-wave radiation scheme (Iacono et al., 2008) and the revised MM5 surface layer scheme (Jiménez et al., 2012).

For the planetary boundary layer, we tested the performance of four different schemes: the Mellor-Yamada-Nakanishi-Niino (MYNN) level 2.5 (Nakanishi and Niino, 2009), the 3DTKE, Shin-Hong scale–aware (SH, Shin and Hong, 2015) and the Yonsei University (YSU, Hong et al., 2006) schemes:

MYNN (Nakanishi and Niino, 2009) scheme belongs to the local closure schemes. It considers local vertical mixing by small eddies and contains prognostic equations for 1-D TKE, predicting SGS turbulence (Saadatabadi et al., 2024; Sathyanadh et al., 2017) as prognostic variable. MYNN has turned out as suitable scheme for wind energy applications in the NEWA study (Hahmann et al., 2020; Dörenkämper et al., 2020) and is to date the only PBL scheme which provides the possibility

https://doi.org/10.5194/wes-2026-103
Preprint. Discussion started: 18 September 2026

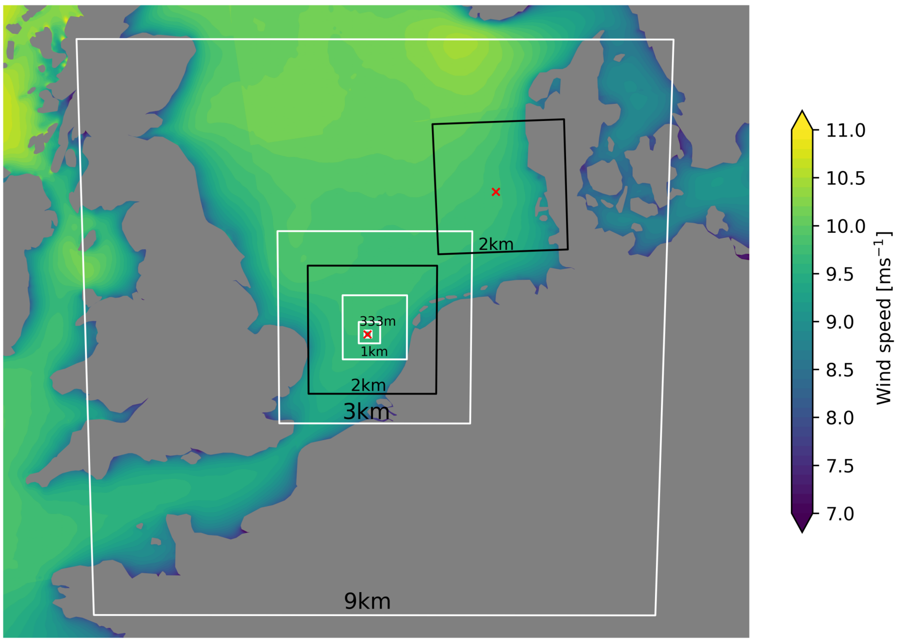

Figure 1. Domain boundaries (white and black polygons) and station location (red x) on top of a regional map with the averaged wind speed in 2013 extracted from the NEWA wind atlas. For IJmuiden, all available inner domains for 3DTKE simulations are shown. For FINO-3, which has been run with its own set of domains, only the 2 km domain is illustrated.

to include wind farm wake effects by the Fitch parameterization (Fitch et al., 2012). It is thus a commonly used PBL scheme in wind energy studies.

YSU (Hong et al., 2006) is also one of the most common PBL schemes as it is able to cope with different atmospheric conditions (Saadatabadi et al., 2024). It is a first order non-local closure scheme considering local and non-local mixing processes within the boundary layer (Saadatabadi et al., 2024; Sathyanadh et al., 2017). However, it does not provide SGS TKE.

SH (Shin and Hong, 2015) is based on YSU and thus a non-local closure scheme with some modification that allow for gray-zone simulations due to a scale-aware PBL option. For larger scales it works similar as YSU. For smaller grid sizes, the local and non-local mixing gets reduced while resolved mixing increases by a fraction consistent with the resolution. TKE is a prognostic variable within this scheme.

3DTKE (Zhang et al., 2018) subgrid mixing, scale-adapting scheme is a newly developed parametrisation (Kilroy et al., 2024) and thus not many studies focusing on hub height wind characterization exist. Like the SH it was developed with the aim of improving gray-zone simulations through a 3 dimensional representation of the length scales needed in a local closure

https://doi.org/10.5194/wes-2026-103
Preprint. Discussion started: 18 September 2026

scheme. Like MYNN it provides the modelled SGS TKE as a direct output variable but contrary to that it combines the horizontal and vertical subgrid turbulent mixing to represent turbulence.

For all simulations, one-way grid nudging was performed and the model was forced by initial and boundary conditions provided by ERA5 (Hersbach et al., 2020) reanalysis and the Operational Sea Surface Temperature and Ice Analysis System (OSTIA) sea surface temperatures (SST, Stark et al., 2007). The model run was conducted for a full year (2013) for all domains running 37 x 10-day-long runs in parallel and an additional spinup time of 24 hours for each 10-day section. For further analysis and the calculation of TI, we extracted the wind component time series from the grid point closest to the respective site of interest from the innermost domains. Results have a temporal resolution of 10 minutes, i.e. every 10 minutes an instant value of each variable has been recorded. Variables have been selected for a couple of vertical levels (heights from ground), which were post-processed through vertical interpolation from the hybrid sigma coordinate system of the WRF model. These heights correspond to the heights for which measurements are available at the respective locations.

Table 2. WRF model setup parameters.

Parameter	**Setting**
WRF model version	4.5
Planetary boundary layer scheme	3DTKE, MYNN, SH, YSU
Surface layer scheme	Revised MM5 Scheme
Land surface model	Unified Noah Land Surface Model
Microphysics scheme	Single-Moment (WSM) 5-class scheme
Radiation schemes	Rapid Radiative Transfer Model for GCMs shortwave and long-wave radiation scheme
Atmospheric boundary conditions	ERA5
Sea surface conditions	OSTIA
Nudging	one way grid nudging
Nesting	one-way
Horizontal resolution	18/6/2 km, 27/9/3/1 km/333/111 m
Vertical resolution	60 eta levels
Temporal resolution output	10-minute

For all runs, we used in addition the provided direct time series output from WRF, which records the temporal highly resolved, instant value of some distinct variables at all selected eta levels for specified locations. This output does not provide TKE but individual wind speed components (u, v, w) at a resolution of a couple of seconds, which helps to derive turbulence intensity based on the wind speeds standard deviation with a temporal resolution comparable to that of measurements. For the evaluation against observations, the data have been resampled to 10 minute averages.

https://doi.org/10.5194/wes-2026-103
Preprint. Discussion started: 18 September 2026

2.1.2 AROME

AROME (Seity et al., 2011; Brousseau et al., 2016) is the mesoscale, limited-area operational model used by Météo-France for numerical weather prediction. It has been shown to provide particularly accurate forecasts of mean wind speed and direction (Jourdier, 2020), but there is no literature focusing on the accuracy of its prediction of turbulent features to our knowledge. In this study, we used the data from the preliminary version of the AROME-reanalysis (ARRA, Bazile et al., 2025). The AROME reanalysis is based on AROME cy48 described in (Brousseau et al., 2016). It uses a horizontal grid spacing of 1.3 km and includes 90 vertical levels, with the lowest level at 5 m above ground level. The domain is centred on France but is relatively large, covering part of the North Sea. IJmuiden is located 379 km from the nearest AROME domain boundary and can therefore be considered unaffected by the simulation's edge effects. The dynamic core of AROME is a semi-implicit, semi-Lagrangian spectral model, which is derived from the IFS/ARPEGE and based on fully compressible system equations. AROME employs the radiation parameterisations of the European Centre for Medium-Range Weather Forecasts (ECMWF). It uses the scheme of Fouquart and Bonnel (1980) for shortwave radiation and the Rapid Radiative Transfer Model (RRTM) code of Mlawer et al. (1997) for longwave radiation. Microphysics are parameterised using a mixed one-moment microphysical scheme (Pinty and Jabouille, 1998). The surface model used is Surfex (Masson et al., 2013). The turbulence in the PBL is represented using an Eddy Diffusivity Mass Flux (EDMF) conceptual scheme, as in the WRF MYNN scheme (Nakanishi and Niino, 2006; Olson et al., 2019). The eddy diffusivity (ED) component is modelled using a prognostic equation for TKE (Cuxart et al., 2000). At a horizontal resolution of 1.3 km, the prognostic equation only considers vertical gradients of the variables and uses the mixing length of Bougeault and Lacarrere (1989). The mass flux (MF) parameterises the contribution of large, anisotropic updrafts to the vertical mixing of variables in the convective PBL Pergaud et al. (2009). The AROME EDMF scheme is that of Pergaud et al. (2009). The current AROME run is initialised and forced at its boundaries by the CERRA reanalysis, which is initialised and forced at its boundaries by ERA5 (Ridal et al., 2024). An incremental analysis updating (IAU) process (Bloom et al., 1996), that is a type of assimilation, is performed every three hours to ensure consistency between AROME and CERRA with regard to mean temperature, humidity and wind field. The AROME outputs used here are taken three hours after the IAU; therefore, the TKE values of AROME are not influenced by the assimilation. Consequently, the TKE values are considered to hinge solely on the physical parameterisation employed in the PBL. The temporal resolution is 1 hour.

2.2 Measurement data

For the evaluation of turbulence intensity derived from both models we used on-site measurement data sets from two publicly available offshore met masts. Besides the high data availability at these two sites shown by Gottschall and Dörenkämper (2021), they provide wind characteristics for two different offshore locations at typical wind exploration areas.

IJmuiden is located in the North Sea, about 85 km off the Dutch coast. It provides wind speed measurements from Thies First Class Advanced cup anemometers at different heights. Here we used 10-minute averages of the horizontal wind speed and its standard deviation from 58 m and 92 m. Observations from the 85 m (cup and Metek USA-1 sonic) anemometer were not used as the data availability was too low with less than 37% at this height. A special quality of the IJmuiden met mast is

https://doi.org/10.5194/wes-2026-103
Preprint. Discussion started: 18 September 2026

Table 3. AROME model setup parameters.

Parameter	**Setting**
AROME model version	cy48
Planetary boundary layer scheme	Eddy Diffusivity Mass Flux conceptual scheme
Surface layer scheme	Surfex (Masson et al., 2013)
Microphysics scheme	mixed one-moment microphysical scheme by Pinty and Jabouille (1998)
Radiation schemes	Rapid Radiative Transfer Model for long-wave radiation and Fouquart and Bonnel (1980) for shortwave radiation
Atmospheric boundary conditions	CERRA reanalysis
Horizontal resolution	1.3 km
Vertical resolution	90 levels
Temporal resolution output	1 hour

that at the same platform, a ground-based ZX lidar with a 50 Hz sampling rate was installed. That allows for a comparison of TI derived from two different measurement devices and adds further heights between 115 m and 215 m. As offshore met mast data are usually not available for heights above 100 m, the lidar provides the possibility to evaluate the model performance beyond the possibilities usually given.

FINO-3 (Bundesamt für Seeschifffahrt und Hydrographie, 2021) [1] is located in the North Sea, about 80 km west of the North-Frisian island of Sylt. It provides wind speed measurements from A100L2 cup anemometers at different heights between 30 m and 106 m. For this study we used 10-minute averages of the horizontal wind speed from 50 m, 60 m, 70 m, 80 m, 90 m, 100 m, and 106 m.

Wind speeds lower than 4 ms^{-1} were excluded from both observations as well as modelled data for the analysis, as typical cut-in wind speeds for wind turbines start between 3-4 ms^{-1} (Saint-Drenan et al., 2020; Maureira Poveda and Wouters, 2015). Furthermore, the steep increase of TI for low wind speeds - as shown in Türk and Emeis (, e.g., 2010) - would skew averages to higher values which on the contrary are not relevant for wind farm operators due to cut-in thresholds. Whenever wind speed was lower in one of the data sets, information from these time steps were completely discarded in all data sets. In met mast data, wind speed was in 10 % of the time stamps below 4 ms^{-1}. Using this condition also including the four different model simulations, in total about 15-17 % of the entire time series are discarded per height. Regardless of discarding these percentage of data, data availability stays above 80% for all heights.

[1]FINO: Forschungsplattform in Nord- und Ostsee - Research platform in the North and Baltic Seas, https://www.fino-offshore.de/de/index.html

2.3 Methods for turbulence intensity calculations

In literature, various methods to calculate turbulence intensity exist. Here, we summarizes the different possibilities which we used in our study. The most commonly used way to calculate TI, in particular for measurements, is based on 10-minute averaged horizontal wind speed (U) and its standard deviation (σ, see, e.g., Tai et al., 2023; Ren et al., 2018; Bodini et al., 2022) as shown in Eq. (1). A slight modification of this formula was suggested by Larsén (2022) who only considers the standard deviation of the along wind component u (Eq. 2).

$$TI_U = \frac{\sigma_U}{\overline{U}} \tag{1}$$

$$TI_u = \frac{\sigma_u}{\overline{U}} \tag{2}$$

An often used method to calculate TI from model data is using the wind flow u- and v-components (Tai et al., 2023) instead of direct wind speed standard deviation as shown in Eq. (3). Mathematically, wind speed and thus its turbulence depends not only on the horizontal but also on the vertical wind component (w). Thus, Siddiqui et al. (2015) calculated wind speed and wind speed deviation based on all three wind speed components and derived TI using Eq. (4).

$$TI_{uv} = \frac{\sqrt{\sigma_u^2 + \sigma_v^2}}{\overline{U}} \tag{3}$$

$$TI_{uvw} = \frac{\sqrt{\frac{1}{3}(\sigma_u^2 + \sigma_v^2 + \sigma_w^2)}}{\overline{U}} \tag{4}$$

TKE (k, Eq. 5) is a parameter - often directly calculated or parametrized in models - that can be used for TI calculation instead of the wind speeds standard deviation. To obtain TI out of TKE we found two suggested equations in literature (see, e.g., Tai et al., 2023; Peña and Mirocha, 2024; Bodini et al., 2020; Khanjari et al., 2025):

$$k = \frac{1}{2}(\sigma_u^2 + \sigma_v^2 + \sigma_w^2) \tag{5}$$

$$TI_{2k} = \frac{\sqrt{2k}}{\overline{U}} \tag{6}$$

$$TI_{2/3k} = \frac{\sqrt{\frac{2}{3}k}}{\overline{U}} \tag{7}$$

3 Results

In this section we show the impact of the PBL scheme and calculation method (3.1), spatial resolution (3.2) and atmospheric stability (3.3) on TI and evaluate results based on observations. Furthermore, the reproducibility of results is proved for a different location (3.4) and a different mesoscale model (3.5).

https://doi.org/10.5194/wes-2026-103
Preprint. Discussion started: 18 September 2026

3.1 Impact of calculation method and PBL schemes

The impact of the calculation method and the performance of each PBL scheme is evaluated here against observed wind speed and TI derived from measurements. For all cases, the 10-minute horizontal wind speeds were used, as commonly provided in observational data sets for wind energy science (MEASNET, 2016). To understand the differences between observations and simulations driven by the use of PBL schemes, an analysis of the underlying components, i.e. the 10-minute average wind speed and its standard deviation has been performed. Figure 2 illustrates both from observations compared to the four modelled ones and Table 4 gives the averaged wind speed and standard deviation of 10-minute intervals over the entire year 2013. As can be seen from Fig. 2, the wind speed distributions tend to be close to each other and there are only small deviations to the observations.

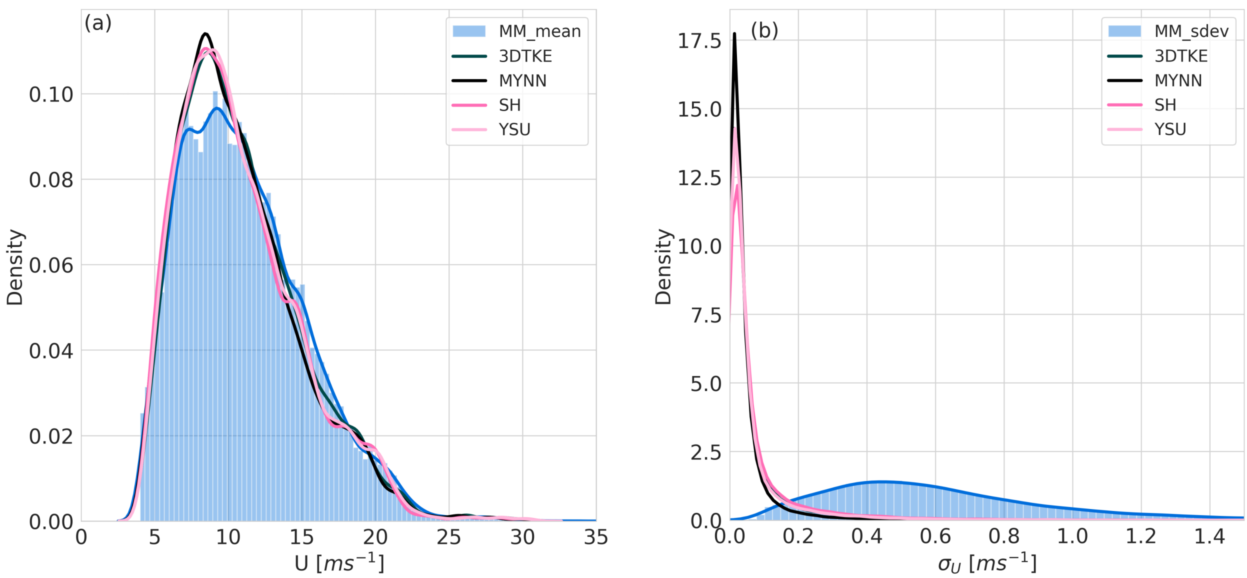

Figure 2. Fitted distribution of wind speed (a) and its standard deviation (b) from met mast observation (MM, blue line with blue filled area) and model simulations using different PBL schemes for IJmuiden at 92 m height for the year 2013. Wind speeds below 4 ms^{-1} were discarded.

The most obvious deviation is a shift towards lower wind speeds resulting in mid-range wind speeds (6-12 ms^{-1}) occurring systematically more often in the model data compared to observations. Contrary to the wind speed, its averaged standard deviation for the 10-minute intervals reveals remarkable differences to observations with a significant and strongly pronounced shift to lower values. These results are further emphasized by the averaged values shown in Table 4: Wind speed averages are close to each other, with the highest bias to observations of 0.44 ms^{-1} for MYNN based simulations, while modelled wind speed standard deviations are about 90 % lower than given in the measurements. A simulation with SH shows the highest standard deviation with 0.08 ms^{-1} per 10-minute interval, while simulations with MYNN reveal the lowest ones.

https://doi.org/10.5194/wes-2026-103
Preprint. Discussion started: 18 September 2026

Table 4. Mean wind speed and standard deviation of the 10-minute intervals at IJmuiden met mast in 92 m height from met mast observations (MM) and PBL scheme based model results as well as RMSE and coefficient of determination (R^2) for the entire year 2013.

	MM	3DTKE	MYNN	SH	YSU
U	11.11	10.88	10.67	10.72	10.80
σ_U	0.62	0.06	0.05	0.08	0.06
RMSE		1.58	1.58	1.61	1.58
R^2		0.86	0.86	0.85	0.86

Hence, with a lower standard deviation and an only slightly lower mean wind speed it can be expected that model-resolved TI is lower than the measured ones. This is in fact visible in Fig. 3, which shows the histograms of modelled and observed TI derived from the various formulas given in Section 2.3.

As has been expected, TI from calculations using any kind of standard deviation (i.e. either standard deviation of the wind speed or standard deviations from different combinations of wind speed components) are much too low compared to observations for all four PBL scheme realizations. Table 5 and Table 6 show the results for mean TI and the RMSE and MAPE for all calculation methods and PBL schemes. All methods based on mesoscale wind fluctuations and model-resolved wind components reveal a similar high RMSE and MAPE with only little variation between the calculation methods and the PBL schemes. For each of these calculation methods, SH has the lowest RMSE and MAPE while for each of the PBL schemes, the method using only the horizontal flow components u and v reveal slightly lower RMSE and MAPE than the other methods. Nevertheless, with RMSE being nearly as high as measured TI as well as with MAPE between 80 and 90 %, results are unsatisfying.

For model simulations using the PBL schemes 3DTKE, MYNN, and SH TKE can be obtained directly from the model. Results for TI using Eq. (6) and Eq. (7) are also shown in Fig. 3 and listed in Tabs. 5 and 6 (lower two rows). The SGS TI calculations using the parameterized TKE from model output represent the observed TI much more realistically, the distribution of the $TI_{2/3k}$ method (Eq. 7) is close to the observed distribution of TI while the TI_{2k} method overestimates observations. All three PBL schemes result in comparable TI when using $TI_{2/3k}$, with 3DTKE and SH showing a slight under- and MYNN an overestimation of TI.

Using parameterized TKE from the model runs and $TI_{2/3k}$ results in a RMSE of 0.024 (3DTKE & MYNN) and 0.027 (SH), respectively as well as a MAPE around 30 % compared to observations. This is a significant improvement to the standard deviation based methods. The Earth Mover Distance (EMD), i.e. the work needed to shift one distribution (model) to the other one (observations) is nevertheless with 0.005 the lowest for MYNN, followed by 3DTKE (0.011) and SH (0.016). Hence, although RMSE is similar and MAPE is slightly worse in MYNN, the distribution is captured slightly better. Using TI_{2k} is not an better option against $TI_{2/3k}$ at mesoscale resolution.

When investigating the observed TI it becomes obvious, that there are some dependencies on season and wind speed itself. The seasonal tendency of TI from measurements shows lower values during spring and summer and higher values in particular during fall (Fig. 4), similar to findings in Bodini et al. (2020) for the US north-east coast. Model-resolved TI does not capture

https://doi.org/10.5194/wes-2026-103
Preprint. Discussion started: 18 September 2026

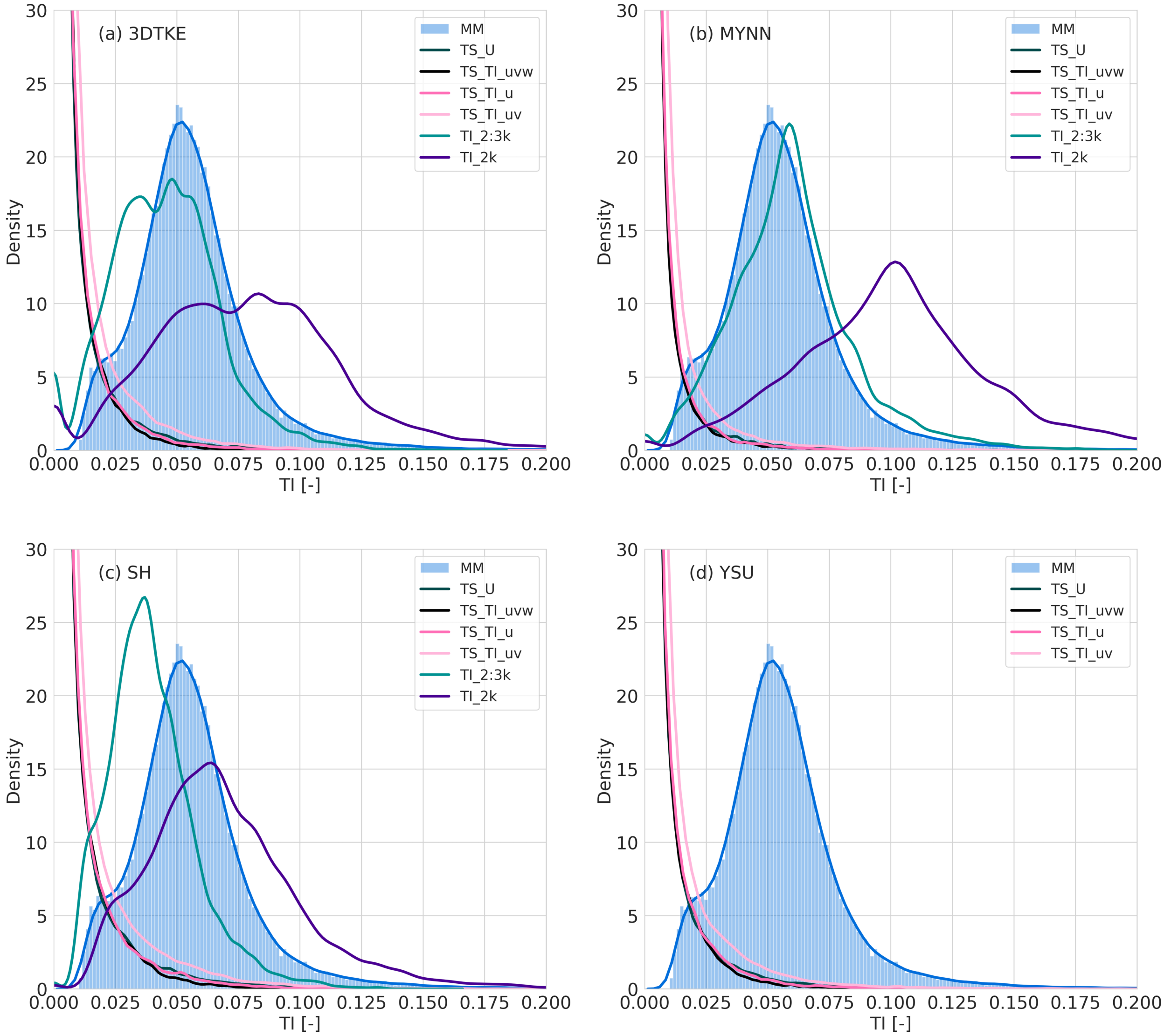

Figure 3. Distribution of TI from observations (blue) and model simulations using different calculation methods and the PBL schemes (a) 3DTKE, (b) MYNN, (c) SH and (d) YSU for IJmuiden at 92 m height for the year 2013.

https://doi.org/10.5194/wes-2026-103
Preprint. Discussion started: 18 September 2026

Table 5. Mean TI from observations and model at IJmuiden at 10 min resolution in time and 92 m height. All model results are taken from a domain with a resolution of 2 km in space.

	MM	3DTKE	MYNN	SH	YSU
TI_U	0.056	0.006	0.005	0.008	0.006
TI_{uvw}		0.006	0.005	0.007	0.006
TI_u		0.006	0.005	0.008	0.006
TI_{uv}		0.010	0.008	0.012	0.010
$\mathrm{TI}_{2/3k}$		0.045	0.060	0.040	
TI_{2k}		0.078	0.103	0.069	

Table 6. RMSE and MAPE between TI from observations and model at IJmuiden at 10 min resolution in time, at 92 m height. All model results are taken from a domain with a resolution of 2 km in space.

	RMSE [ms^{-1}]				MAPE [%]			
	3DTKE	MYNN	SH	YSU	3DTKE	MYNN	SH	YSU
TI_U	0.056	0.057	0.055	0.056	88.6	90.8	86.4	88.6
TI_{uvw}	0.056	0.057	0.055	0.056	89.1	91.1	86.9	89.1
TI_u	0.056	0.057	0.055	0.056	88.6	90.8	86.4	88.5
TI_{uv}	0.053	0.055	0.052	0.054	82.8	86.0	80.3	83.0
$\mathrm{TI}_{2/3k}$	**0.024**	**0.024**	0.027		**29.5**	33.3	32.2	
TI_{2k}	0.038	0.060	0.03		56.4	102.3	43.9	

this seasonal cycle while SGS TI tend to follow the observations. Again, TI derived using Eq. (6) (TI_{2k}) shows generally an overestimation, while TI derived from Eq. (7) is closer to observations, slightly more for MYNN than for 3DTKE and SH. In all cases $TI_{2/3k}$ captures the variance between months realistically, while TI_{2k} overestimates also the seasonal variability. However, for 3DTKE (SH) TI_{2k} shows a higher agreement for the months from April to June (Juli) than $TI_{2/3k}$. This highlights the importance of investigating full years or even longer periods, as such variability might not have been found from short-term investigations.

Former studies showed that turbulence has also an effect on power curves in the vicinity of rated wind speeds (e.g. Sheinman and Rosen, 1992; Rosen and Sheinman, 1994; Kaiser et al., 2007; Albers et al., 2007; Wharton and Lundquist, 2012a; Bardal and Sætran, 2017). Hence, we investigated as to whether TI dependency on wind speed can be reflected in the model simulations. Figure 5 illustrates that observed TI first decreases with increasing wind speeds until it reaches a minimum in the area of rated wind speeds and starts to increase for moderate to high wind speeds. $TI_{2/3k}$ is for 3DTKE and MYNN close to observations at lower wind speeds, but at wind speeds higher than 15 ms^{-1} the deviation between observations and modelled TI increases, for 3DTKE more than for MYNN. SH is again similar to 3DTKE, with TI slightly shifted towards lower values so that observations are more or less between $TI_{2/3k}$ and TI_{2k}, with $TI_{2/3k}$ showing an under- and TI_{2k} an overestimation

https://doi.org/10.5194/wes-2026-103
Preprint. Discussion started: 18 September 2026

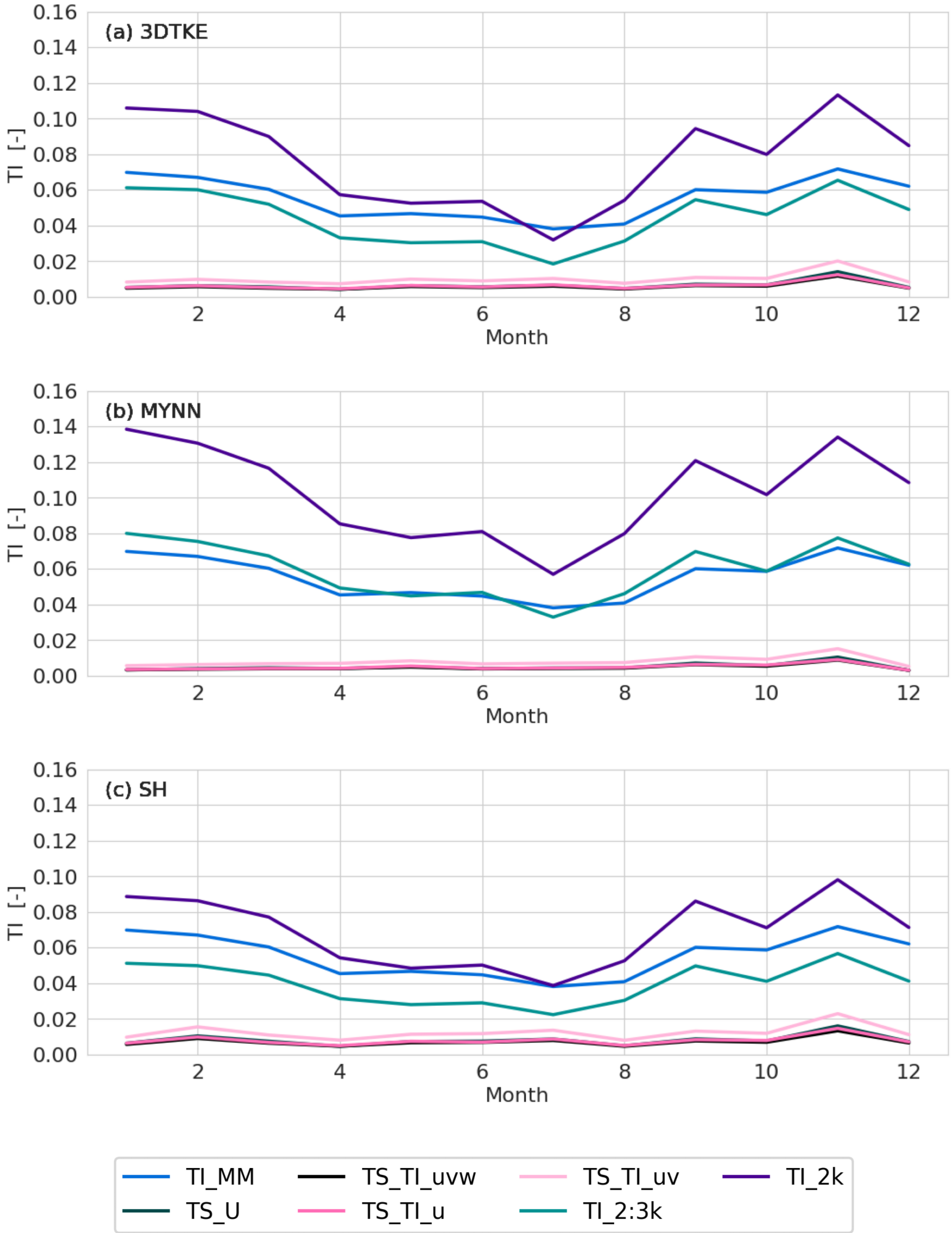

Figure 4. Seasonal cycle of TI from observations compared to model-resolved and SGS model results.

https://doi.org/10.5194/wes-2026-103
Preprint. Discussion started: 18 September 2026

of observed TI. For TI_{2k} the general overestimation decreases with increasing wind speed. Hence, the observed shape of TI vs wind speed dependency is not fully captured by none of the three PBL schemes. However, the model-resolved TI cannot reflect the observed behaviour of TI over wind speed at all, instead it tend to further decrease with increasing wind speeds for all PBL schemes and calculation methods.

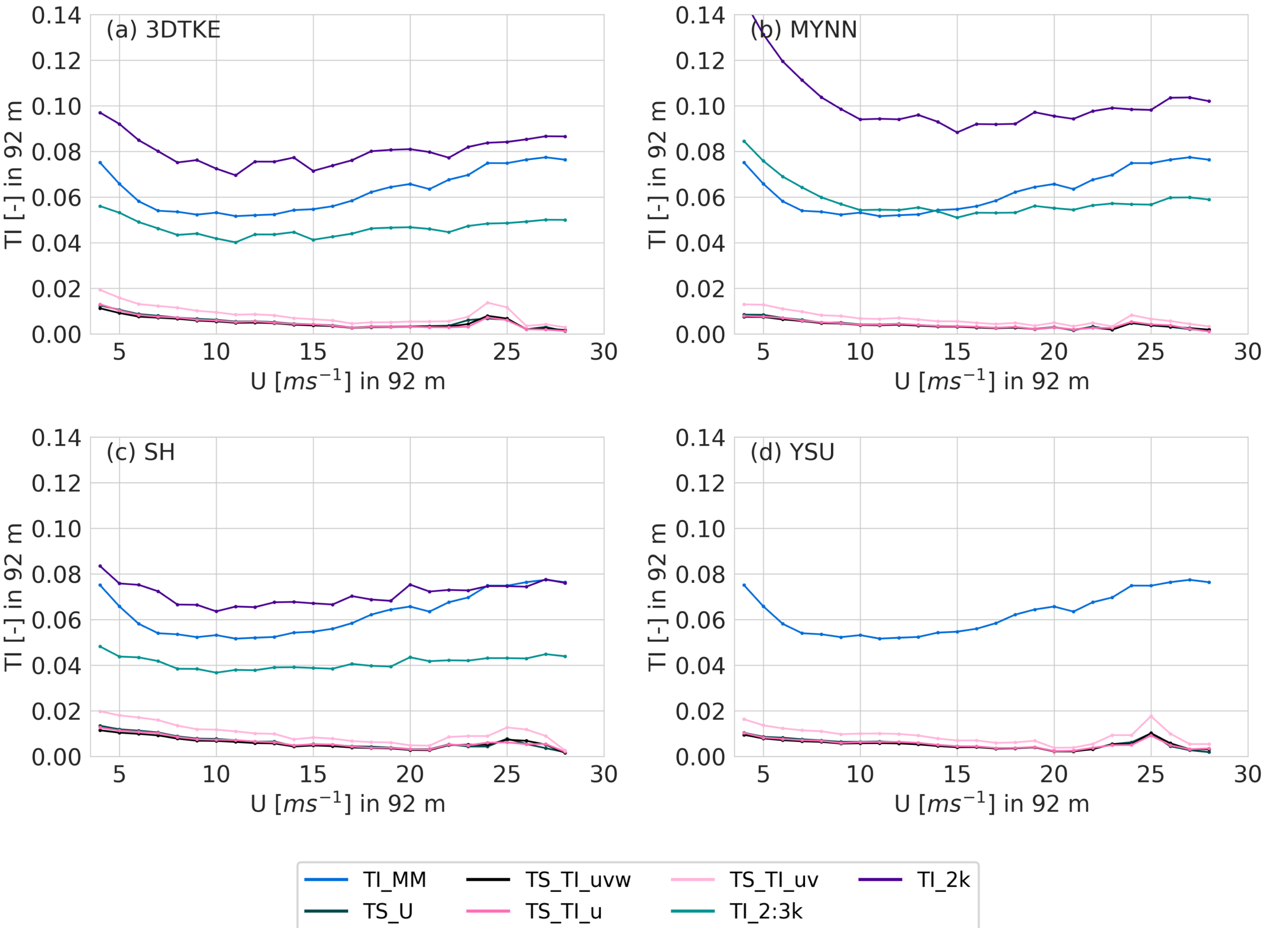

Figure 5. Wind speed dependent TI for a) 3DTKE, b) MYNN, c) SH and d) YSU for SGS and model-resolved TI.

Results shown here are all based in comparisons at 92 m height. However, all calculations have been done at further heights from which met mast data are available (not shown) but no significant differences to the discussed results could be found.

Summarized, over a full year, results indicate that the parametrized TKE output from model simulations provides more reliable TI values and is a suitable option as they show the lowest deviation to observations compared to model-resolved methods. These findings align with the fact that wind turbulence occurs on smaller scales than a mesoscale model can resolve.

https://doi.org/10.5194/wes-2026-103
Preprint. Discussion started: 18 September 2026

The performance of the different PBL schemes is similar over a full year at a 2 km resolution with a common MAPE around 30%.

3.2 Spatial resolution effect

As WRF provides the option to perform simulations on gray-zone resolutions, we investigated the potential of it to provide TKE on scales smaller than usually used in mesoscale studies and to analyse as to weather gray-zone simulations might become a cost efficient bridge between mesoscale and LES simulations. The 3DTKE and SH PBL schemes have been designed to be also used in the gray zone (100 - 1000 m). Therefore we performed a simulation with these PBL schemes on six domains, with a resolution factor of 3 for each domain, starting from 27 km for the outermost to 1 km, 333 m and 111 m for the innermost domains. Fig. 6 shows the TI distribution for the three innermost domains compared to TI from 2 km resolved model simulations for SGS TI from both simulations and Tables 7 and 8 list mean values and RMSE, MAPE and EMD between modelled and observed TI at mesoscale and gray-zone resolutions, respectively.

Wind speeds show only very slight and no consistent changes over the different resolutions and compare well with the averaged wind speed of 11.1 $\mathrm{m\,s^{-1}}$ in observations. SGS TI, on the contrary, decreases on average with increasing resolution, driven by the decrease in TKE. For $TI_{2/3k}$, this decrease results in further underestimation of observed TI while for TI_{2k}, the distribution comes closer to the observed one. SH providing the best result for a resolution of 111 m using TI_{2k}. Contrary to the decrease in TKE within the model simulations, the 10-minute standard deviation increases with increasing spatial resolution. This increase is expected as more parts of the turbulent fluctuations are getting resolved by the finer grid resolution. However, at 111 m, the modelled wind speeds standard deviation is with 0.14 $\mathrm{m\,s^{-1}}$ (0.16 $\mathrm{m\,s^{-1}}$) for 3DTKE (SH) still far lower than the observed standard deviation of 0.62 $\mathrm{m\,s^{-1}}$.

Hence, even with resolutions in the gray zone, WRF cannot simulate the standard deviation and accordingly model-resolved TI adequate enough. Although TI increases by a factor of 3 from 3 km (0.005-0.01) to 111 m (0.014 to 0.028) it is still much lower than what SGS TI provides (not shown). Using the parameterized SGS TKE results in better TI agreement between model and observations, but the way of TI calculation from TKE depends on the spatial resolution. For $TI_{2/3k}$, the highest comparability to observations is gained at resolutions of 2-3 km. With increasing resolution, TI decreases as SGS TKE does, and thus deviates stronger to the observed averaged TI of 0.56. For TI_{2k}, the closest TI value is reached at a resolution of 111 m. With a value of 0.063, TI is 0.007 higher for 3DTKE than for observation. SH reaches an averaged TI of 0.056 at this resolution, which is identical to averaged TI from observations. Thus, the results indicate that with increasing resolution, TI_{2k} becomes the better way for TI calculations, in particular for simulations with SH.

Figure 7 illustrates the dependency of TI on wind speed and the difference between two spatial resolutions. While at 2 km resolution $TI_{2/3k}$ captures observation in the area below 15 $\mathrm{m\,s^{-1}}$, it tends to underestimate TI increasingly with increasing wind speeds beyond 15 $\mathrm{m\,s^{-1}}$ for 3DTKE. For SH, observations are between both calculation methods for wind speeds below 15 $\mathrm{m\,s^{-1}}$. Above 15 $\mathrm{m\,s^{-1}}$ TI_{2k} comes closer to observation for both PBL schemes. For a 111 m resolution, TI_{2k} becomes overall the more accurate method. It shows only a slight overestimation for lower wind speeds and a slight underestimation for wind speeds higher than ≈17 $\mathrm{m\,s^{-1}}$ at this resolution. The model-resolved methods move closer to observations with increased

https://doi.org/10.5194/wes-2026-103
Preprint. Discussion started: 18 September 2026

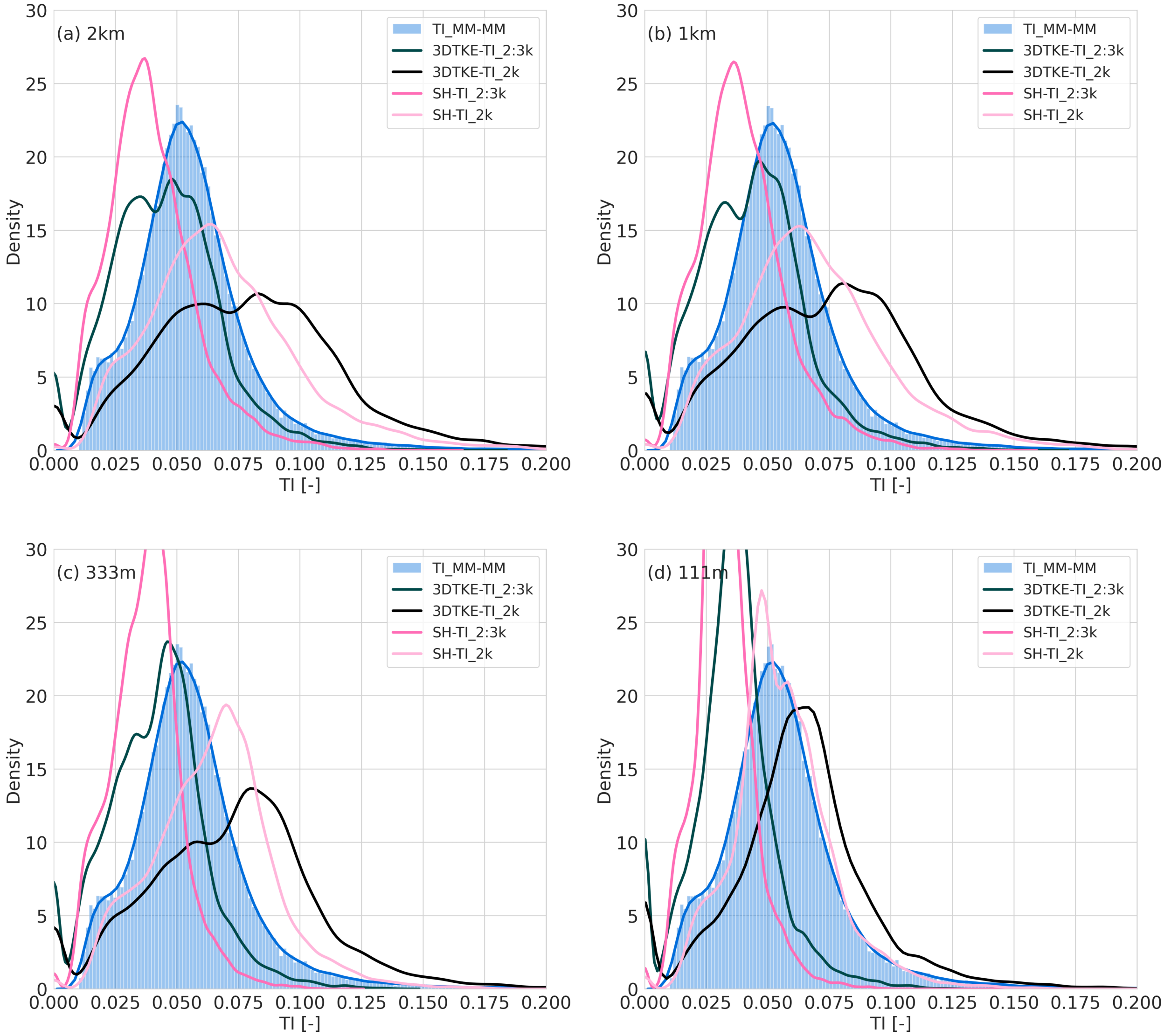

Figure 6. TI distribution obtained from 3DTKE simulation at spatial resolutions of (a) 2 km, (b) 1 km, (c) 333 m, and (d) 111 m at IJmuiden met mast (blue) and 92 m height compared to measurements.

https://doi.org/10.5194/wes-2026-103
Preprint. Discussion started: 18 September 2026

Table 7. Mean wind speed, standard deviation, TKE and turbulence intensity from 3DTKE and SH driven model simulations at IJmuiden and 92 m height for different spatial resolutions.

	3 km	2 km	1 km	333 m	111 m
3DTKE					
U	10.9	10.9	11.0	11.0	10.9
σ_U	0.05	0.06	0.09	0.12	0.14
k_{SGS}	0.453	0.453	0.419	0.386	0.283
$TI_{2/3k}$	**0.045**	**0.045**	0.043	0.041	0.036
TI_{2k}	0.078	0.078	0.074	0.072	0.063
SH					
U	10.8	10.8	10.7	10.7	10.6
σ_U	0.06	0.08	0.10	0.14	0.16
k_{SGS}	0.345	0.341	0.339	0.298	0.212
$TI_{2/3k}$	0.040	0.040	0.040	0.037	0.032
TI_{2k}	0.070	0.069	0.069	**0.065**	**0.056**

Table 8. RMSE, MAPE and EMD between 10-minute TI from observations and 3DTKE and SH driven model at IJmuiden, 92 m height for 1 km and 333 m resolution in model simulations.

	RMSE [ms^{-1}]		MAPE [%]		EMD	
	1 km	111 m	1 km	111 m	1 km	111 m
3DTKE						
$TI_{2/3k}$	**0.025**	0.029	**31.7**	36.7	**0.013**	0.020
TI_{2k}	0.036	0.027	52.5	39.2	0.020	**0.009**
SH						
$TI_{2/3k}$	0.027	0.032	32.0	40.1	0.016	0.024
TI_{2k}	0.030	**0.023**	44.4	**30.4**	0.014	**0.002**

https://doi.org/10.5194/wes-2026-103
Preprint. Discussion started: 18 September 2026

spatial resolution, but still show a strong underestimation of TI. Hence, TI may be represented slightly more precisely when increasing the resolution to 111 m and changing the calculation method from $TI_{2/3k}$ to TI_{2k}. However, MAPE is in any case around 30%.

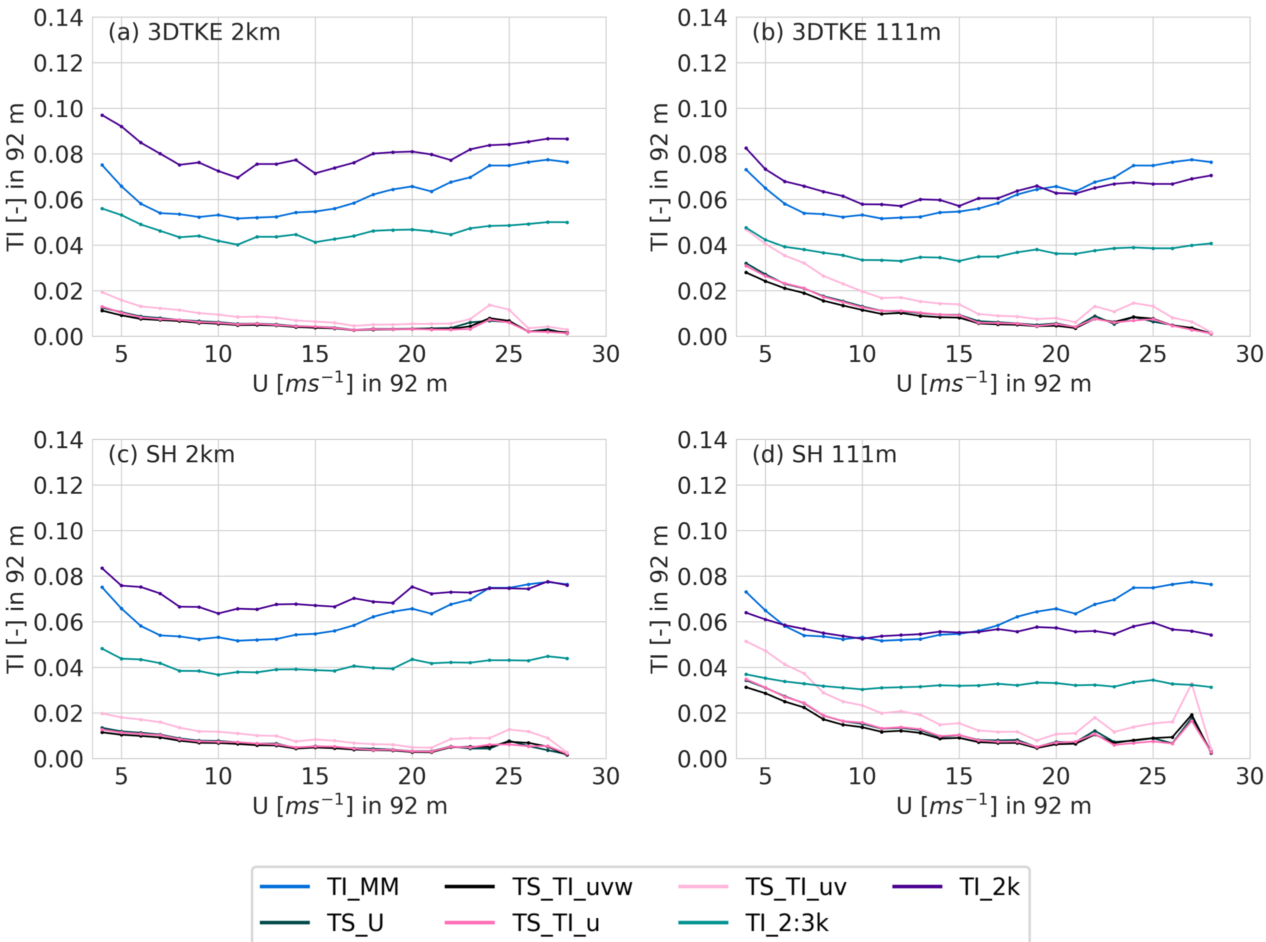

Figure 7. TI vs wind speed for 3DTKE (top) and SH (bottom) simulations at 2 km (a, c) and 111 m (b, d) spatial resolution compared to observations at met mast IJmuiden (blue) at 92 m height.

3.3 Quantification of TI under varying atmospheric stability

In order to assess the models performance under varying atmospheric stabilities we divided the data into three categories: stable, unstable and neutral. For the stability classification the - by the WRF model - calculated Reverse Monin-Obukhov length has been used and thresholds follow those suggested in Archer et al. (2016) (neutral: $|L| > 500$, stable: $L = 5$ to 500, unstable: $L = -5$ to -500). About 9-17 % of the data fall into the category of neutral conditions for all PBL schemes. For stable and unstable data, the amount of data varies between the PBL schemes (see Table 9).

Table 9. Amount of data in % per stability category and PBL scheme.

	neutral	stable	unstable
3DTKE	17 %	47 %	36 %
MYNN	11 %	39 %	50 %
SH	9 %	59 %	32 %

The evaluation was then performed over several heights, which has been done by including the lidar data from IJmuiden. First of all, a difference in met mast and lidar data based TI can be identified (see Fig. 8a), which has already been mentioned in Maureira Poveda and Wouters (2015). The lidar data show an obvious shift towards higher TI compared to met mast data. Furthermore, the increase in TI over height shown in the lidar data is not expected, as the turbulence generally decreases with increasing height. Due to the different measurement principle of a lidar, including the varying temporal and spatial resolution, errors in the measurements may also increase over height (see, e.g., Robey and Lundquist, 2022; Newman et al., 2016; Sathe and Mann, 2013). The driving factor in the difference between met mast and lidar is here the standard deviation, which is higher for lidar data and reveals a similar shift as TI does (not shown).

Given the fact, that there are already deviations between both measurement devices, an absolute conclusion about a correct model simulation over all heights cannot be given here as this would need further data with more heights than available for this study to verify the correctness of the lidar data. Nevertheless, the models variability in TI under varying atmospheric stability is further investigated here and is related to the variability reflected by both devices over the respective heights.

In case no stability separation has been performed (Fig. 8 a) $TI_{2/3k}$ represents met mast observations best, while the lidar data at higher heights are better represented by TI_{2k}, for a simulation with 3DTKE. For simulations with MYNN, $TI_{2/3k}$ reveals mean TI between both observational data sources. The variation in modelled TI over height agrees well with met mast results for both PBL schemes. The increase in TI over height observed by the lidar data is - as expected - not given in model simulations which instead reveal a decrease in TI over height. This reflects how variable results may become under varying constellations of model simulations and also observations taken for evaluations. Figure 8 b-d) compares furthermore TI averaged over all atmospheric stabilities (Fig. 8a) with TI for neutral (Fig. 8b), stable (Fig. 8c) and unstable (Fig. 8d)) conditions for the different PBL schemes.

For neutral conditions, $TI_{2/3k}$ underestimates and TI_{2k} overestimated TI for a simulation with a spatial resolution of 2 km and using 3DTKE or SH as PBL scheme. MYNN captures TI overall best with only a slight underestimation with $TI_{2/3k}$. During stable conditions, TI is generally on average lower. For these cases, TI_{2k} is closer to the met mast values than $TI_{2/3k}$ and the development over height is not well represented. All methods reveal a stronger decrease over height than reflected by the observations. Under unstable conditions, TI is on average the highest and $TI_{2/3k}$ results again in more accurate TI values.

https://doi.org/10.5194/wes-2026-103
Preprint. Discussion started: 18 September 2026

For 3DTKE, met mast and model simulated mean TI are nearly the same. TI_{2k} shows again a strong overestimation compared to met mast data.

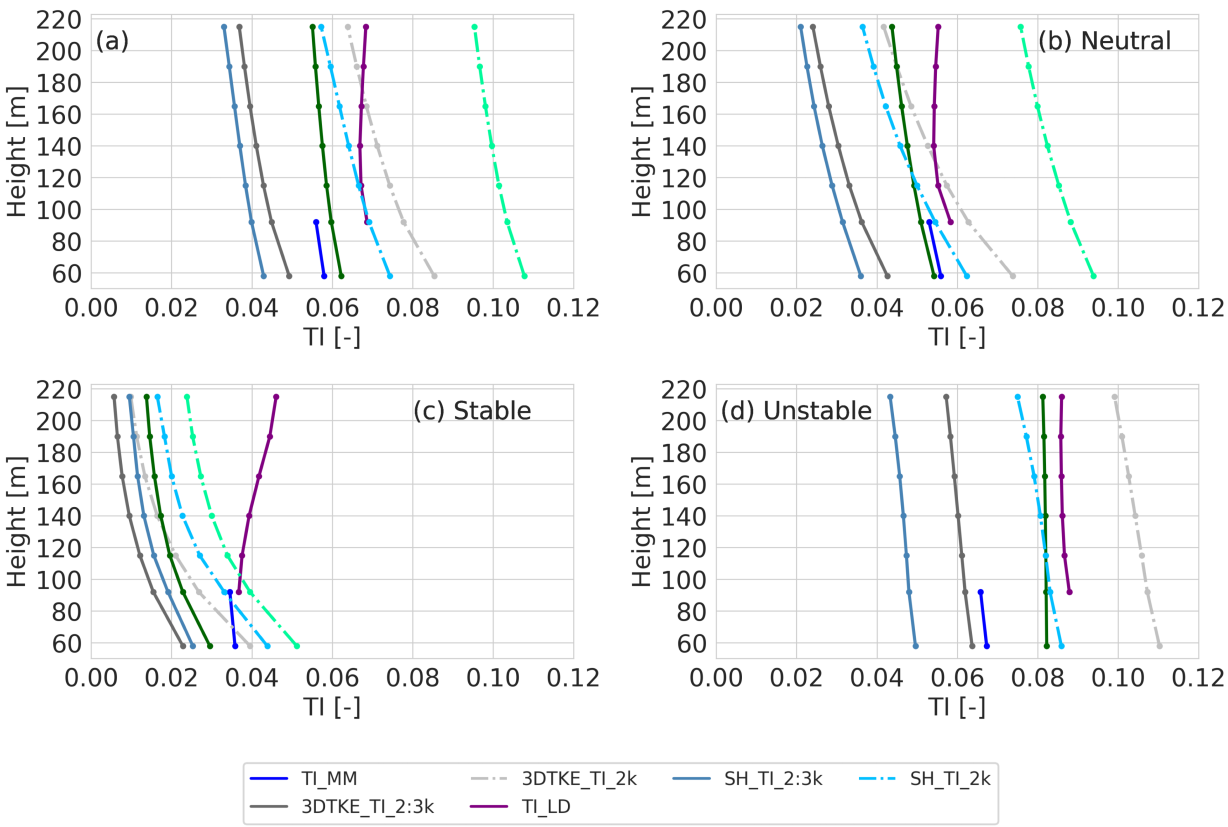

Figure 8. TI at different heights from observations (blue: anemometer (MM), purple: lidar (LD)) for SGS scale methods at IJmuiden for all data (a) no stability separation, b) neutral, c) stable, and d) unstable conditions.

Overall, MYNN with $TI_{2/3k}$ is in general closest to observations and the slight overestimation shown in Fig. 8 a) results from the strong overestimation during unstable conditions and a slight underestimation during the other cases. This implies that a better representation of unstable turbulence processes within the PBL scheme might improve the overall turbulence intensity. 3DTKE is on the other hand best for unstable conditions while in all other cases it reveals a strong underestimation of turbulence intensity.

3.4 Verification of results at FINO-3

In order to verify that results found for IJmuiden are valid also for other locations in the North Sea, the same calculations were done at FINO-3, shown here for the 2 km spatial resolution. Mean wind speed from met mast was $11.2 \pm 0.6\,\mathrm{ms^{-1}}$ at 90 m

https://doi.org/10.5194/wes-2026-103
Preprint. Discussion started: 18 September 2026

height in 2013, slightly higher than for IJmuiden at 92 m height for the same year ($11.1 \pm 0.62\,\mathrm{ms^{-1}}$). The averaged TI out of the 10-minute mean wind speeds and standard deviations was 0.059, also slightly higher than observed at IJmuiden (0.056).

Table 10 lists the corresponding mean values for wind speed, standard deviation, TKE and TI from the various calculation methods.

Table 10. Wind speed, standard deviation and mean, RMSE, and MAPE between 10-minute TI from observations and mesoscale model results using the 3DTKE/MYNN/SH PBL schemes at FINO-3, 90 m height. All model results have an underlying horizontal resolution of 2 km.

	Mean [$\mathrm{ms^{-1}}$]			RMSE [$\mathrm{ms^{-1}}$]			MAPE [%]		
	3DTKE	MYNN	SH	3DTKE	MYNN	SH	3DTKE	MYNN	SH
U	11.1	10.9	11.0	1.70	1.66	1.68	12.5	12.2	12.4
σ_U	0.08	0.05	0.09	0.71	0.74	0.70	86.8	90.7	85.2
k_{SGS}	0.454	0.676	0.347	0.720	0.695	0.800	67.0	137.6	58.6
TI_U	0.008	0.005	0.009	0.062	0.064	0.061	86.7	90.4	85.0
TI_{uvw}	0.007	0.005	0.008	0.062	0.064	0.061	87.2	90.4	85.2
TI_u	0.008	0.006	0.009	0.062	0.063	0.061	86.6	90.0	84.8
TI_{uv}	0.012	0.009	0.014	0.059	0.062	0.058	80.7	85.4	78.8
$TI_{2/3k}$	0.046	0.060	0.041	0.033	0.032	0.035	31.3	37.8	33.6
TI_{2k}	0.079	0.103	0.070	0.042	0.061	0.037	60.6	105.6	49.2

In summary, the FINO-3 results support all findings from the IJmuiden analysis:

1. The standard deviation from the temporal highly resolved time series output is much lower than standard deviation from observations. This holds for all three PBL scheme realizations.
2. The model-resolved TI is therefore also ways to low compared to observations. MAPEs are within a similar range than found for IJmuiden.
3. TI based on SGS TKE is significantly closer to observations than model resolved TI.
4. Using 3DTKE reveals similar deviations in terms of RMSE as MYNN and the lowest MAPE.
5. MYNN, however, shows the lowest bias to mean TI from observations.
6. Calculations with Eq. (7) ($TI_{2/3k}$) result in lower RMSE and MAPE between model and observations than those with Eq. (6) (TI_{2k}).

Figure 9 visualizes the similarity of results for both locations (a) IJmuiden and b) FINO-3 in terms of mean TI over height. We conclude from these findings that over the here presented calculation methods $TI_{2/3k}$ (Eq. 7) at a spatial resolution of 2 km and a temporal resolution of 10 minutes reveals the lowest deviations to observations. Out of the used PBL schemes,

https://doi.org/10.5194/wes-2026-103
Preprint. Discussion started: 18 September 2026

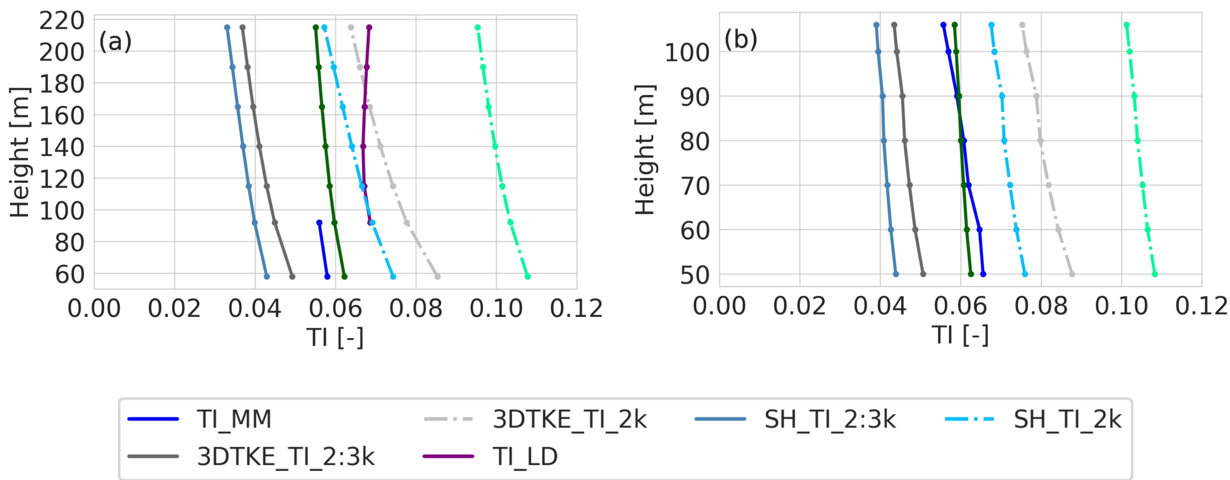

Figure 9. Comparison of TI at different heights at a) IJmuiden and b) FINO-3 from observations (blue: anemometer (MM), purple: lidar (LD)) for SGS methods. Note the different scaling of the vertical axes.

MYNN provides the closest averaged TI to observations at a resolution of 2 km. However, in case that computational costs do not limit the calculation process, TI_{2k} may also become a reasonable methods at higher gray-zone resolutions, in particular when using SH as PBL scheme. On the contrary, results indicate that model-resolved TI (i.e. based on standard deviation of wind speed or wind speed components) from WRF mesoscale and gray-zone simulations are not an appropriate option to represent turbulence intensity in the North Sea. This limits the available PBL schemes for simulations to those providing TKE.

3.5 Sensitivity study with AROME

To verify the findings from the WRF simulations and ensure that these are in generall independent from the kind of mesoscale model, we compared TI and TKE from WRF with output from AROME. At the IJmuiden site AROME results are available for the horizontal wind speed components u and v as well as for TKE at 1h resolution and TI has been calculated from these instant 1h values. For the comparison with WRF and observations, 1h instant values have been extracted from these data sets as well. Thus, results are not explicitly comparable to the above described results. They rather aim to reflect potential differences and similarities in mesoscale model results. As TI from Eq. (7) revealed the most promising results for simulations within the mesoscale resolution in this study, we used only this equation for our comparison with AROME. Accordingly, WRF results from 3DTKE, MYNN and SH are considered here.

Figure 10 shows how wind speed, TKE and TI compare between AROME, WRF and observations at IJmuiden at a height of 92 m. The distribution of wind speed from AROME seems to be closer to observations than those from the WRF simulations. This behaviour is to be expected since the mean wind fields of AROME are subject to IAU, which is a type of assimilation (see Section 2.1.2). However, also the WRF wind speed distributions do not deviate strongly from observations at all. Mean values

https://doi.org/10.5194/wes-2026-103
Preprint. Discussion started: 18 September 2026

deviate by 0.07 ms^{-1} (AROME) to 0.47 ms^{-1} (WRF-MYNN), as shown in Table 11. RMSE between model simulations and observations amount to 1.4 ms^{-1} (AROME), 1.6 ms^{-1} (WRF-3DTKE and WRF-MYNN) and 1.7 ms^{-1} (WRF-SH). Hence, wind speed seems to be reflected well in all model simulations.

400 Despite the similarity in wind speed distribution, TKE shows significant differences between the model realizations, with TKE in MYNN being the highest and in SH and AROME the lowest (see Table 11). Finally, TI is underestimated from SH, AROME and 3DTKE but slightly overestimated by MYNN (see Fig. 10 c).

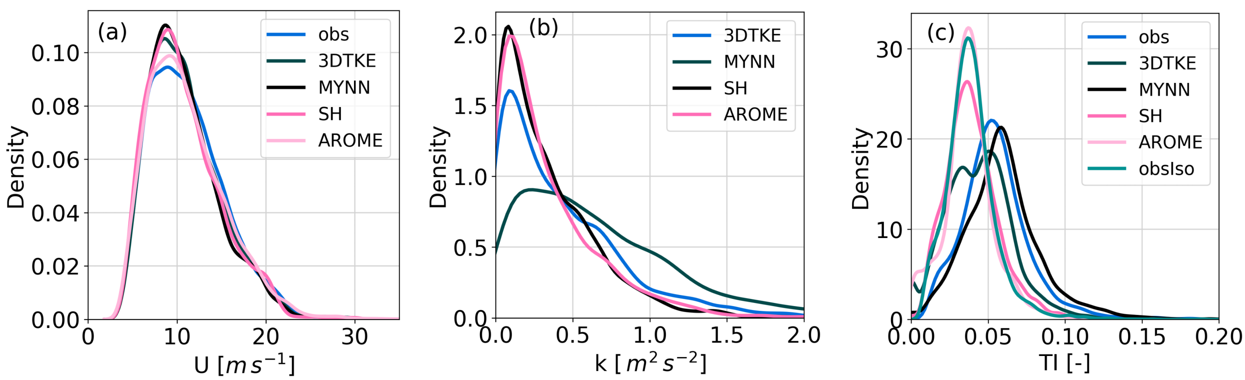

Figure 10. Mesoscale model intercomparison: 1h instant AROME and WRF wind speed, TKE and TI evaluated against observations at IJmuiden met mast at 92 m hight and a spatial resolution of 2 km.

As the deviation from AROME TI to observations is the strongest, we tested also the performance of Eq. (6), i.e. using a factor of 2 instead of 2/3, which is often used for LES based simulations. This test results in a TI value of 0.065, which is higher

405 than the observed TI. RMSE and MAPE are still higher than for the simulation with WRF using the 3DTKE PBL scheme. Thus, using Eq. (6) cannot improve the results.

Table 11. Mean, RMSE, and MAPE between 1h instant wind speed, TKE and TI from observations and 3DTKE, MYNN and SH driven WRF simulations compared to AROME at 92 m height for 2 km resolution in model simulations.

	obs	AROME	3DTKE	MYNN	SH
U [ms^{-1}]	11.25	**11.18**	11.03	10.78	10.85
k_{SGS} [-]	-	0.353	0.439	0.686	**0.346**
TI [-]	0.055	0.038	0.044	**0.060**	0.040
MAPE TI [%]	-	32.5	**30.2**	32.7	31.1

This comparison indicates that neither the hourly resolution nor using another mesoscale model with a different setup significantly change the results found in this study: With the mesoscale model approach and using SGS TKE for TI calculation, averages with a MAPE of about 30% can be achieved for the North Sea.

https://doi.org/10.5194/wes-2026-103
Preprint. Discussion started: 18 September 2026

Open Access WIND ENERGY SCIENCE DISCUSSIONS

4 Discussion

This study showed that TI from mesoscale simulations deviate to some degree from observations. A potential source of errors might be due to different temporal resolutions. The observational data have a sampling frequency of seconds, which are resampled to 10-minute averages. Records of TKE from the mesoscale models are instant 10-minute values and thus do not consider deviations within the 10-minute intervals considered in observations. To identify the impact of this temporal deviation, a one month simulation at 1-minute resolution was performed with MYNN. These 1-min records were resampled to 10-minute averages and are compared to observations. As can be seen in Fig. 11, TI resulting from 1-min simulations does rarely deviate from TI out of 10-minute instant values. A difference in mean TI between both resolutions only occurs in the 5th decimal place. Hence, increasing the temporal resolution would result in higher computational costs but not in an improved representation of TI in mesoscale models, which are not able to reflect these high resolution processes.

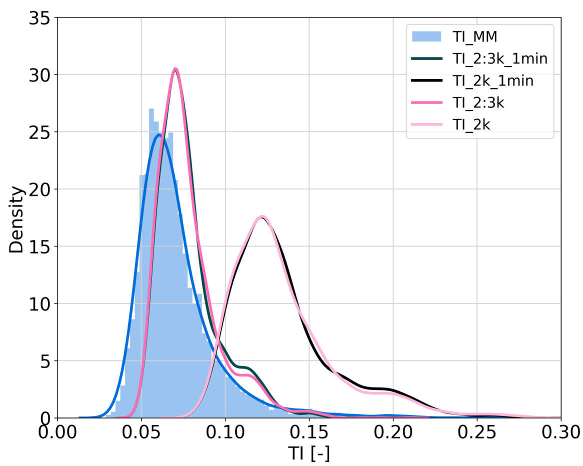

Figure 11. SGS TI from 10-minute instant TKE and wind speed records and 10-minute averages from 1-min resolved TKE and wind speed.

Another aspect to consider is that TI performance in WRF was throughout the paper analyzed by using SGS and model-resolved TI separately. Peña and Mirocha (2024) combined both parts in their WRF-LES studies to a total TI, which raises the question as to whether the comparisons in this analysis are lacking a fully resolved turbulence. Thus, we proofed the potential of summing up the SGS TI from Eq. (7) and the model-resolved TI to a total TI using all the available formulations. Table 12 lists results for mean, RMSE and MAPE referred to observations (TI_{MM} = 0.056) from the SGS TI from Eq. (7) and the total TI.

For 3DTKE, mean total TI is much closer to observations (0.056) than the SGS TI (0.045), with a RMSE that is similar for all cases and a MAPE that deviates only slightly. EMD decreases but the correlation becomes worse (not shown). Hence, through the combination of both scales, TI becomes on average higher and the distribution closer to that of observations. Nevertheless, the amount of deviations is still the same with a MAPE of around 30%. With higher resolutions (up to 111 m), mean TI stays closer to that of observations for total TI but RMSE and MAPE become worse. With MYNN, which shows

https://doi.org/10.5194/wes-2026-103
Preprint. Discussion started: 18 September 2026

Table 12. Mean total TI (SGS plus model-resolved) and RMSE and MAPE between 10-minute TI from observations and 3DTKE, MYNN and SH at IJmuiden at 92 m height for 2 km resolution in model simulations.

	Mean [ms^{-1}]			RMSE [ms^{-1}]			MAPE [%]		
	3DTKE	MYNN	SH	3DTKE	MYNN	SH	3DTKE	MYNN	SH
TI$_{2/3k}$	0.045	0.060	0.040	0.024	0.024	0.027	29.5	33.3	32.2
TI$_{Utot}$	0.051	0.065	0.048	0.024	0.027	0.026	30.4	38.2	32.2
TI$_{uvwtot}$	0.051	0.064	0.047	0.024	0.027	0.025	29.3	37.6	30.9
TI$_{utot}$	0.051	0.065	0.048	0.024	0.027	0.026	30.0	38.1	31.8
TI$_{uvtot}$	0.055	0.068	0.052	0.026	0.030	0.028	32.1	42.1	34.3

already an overestimation in the SGS TI, a combination with the model-resolved TI results in an even higher deviations. Thus, for this PBL scheme, calculation of total TI does not improve the outcome. SH simulations showed the lowest SGS TI and improves when combining it with model-resolved TI. Nevertheless, TI is still lower than 3DTKE results and RMSE and MAPE is slightly higher compared to 3DTKE. Summarized, combining the model-resolved and SGS TI is not a general solution to fully depict observed TI and therefore additional or other improvements are required to obtain more reliable TI from the mesoscale simulations.

5 Conclusions

The focus of this study was to evaluate the possibilities and limitations of representing TI for offshore wind site assessment in the North Sea using WRF. WRF simulations were performed using 4 different PBL schemes at two locations and up to 5 spatial resolutions between 3 km and 111 m for the full year of 2013. As various different calculation methods for TI were found in literature, we compared these options in order to identify an optimal combination of WRF PBL parameterization and TI calculation method. The impact of atmospheric stability has been studied and it has been discussed to which extent temporal resolution and a combination of SGS and model-resolved TI could affect results. Furthermore we addressed the challenges in evaluating model results against different measurement devices and verified results by a comparison with another mesoscale model. The study identified that while simulated wind speed is generally well represented, its fluctuation reveals noticeable differences to observations with a significant and strongly pronounced shift to lower values. This results in a poor representation of model-resolved TI, which is calculated using the wind speeds standard deviation, with absolute percentage errors of 80-90%. Out of the four PBL schemes analyzed, Shin-Hong (SH) has the lowest and MYNN the highest deviations. With higher resolutions, standard deviation of the 10-minute intervals increases slightly but not strong enough to result in TI comparable to observations. By using the SGS TKE from simulations with 3DTKE, MYNN, and SH, TI values improve significantly compared to model-resolved TI. In general, $TI_{2/3k}$ provides values closer to observations than TI_{2k}. However, there are variations in the seasonal cycle, stability effects and spatial resolution which may force TI_{2k} to become as good or even more precise. Nevertheless, both methods still result in RMSE from 0.024-0.060 and a MAPE of about 30% for the best

https://doi.org/10.5194/wes-2026-103
Preprint. Discussion started: 18 September 2026

cases independent of the spatial resolution, measurement location, used PBL scheme and used mesoscale model. Thus, for any further improvement either LES simulations or a kind of correction method like Measure-Correlate-Predict (MCP) becomes necessary.

Author contributions. SaS designed the experiment, conducted the WRF mesoscale model simulations, generated the results, and wrote and edited the manuscript. TL provided AROME data, contributed to writing the manuscript and conducted extensive discussion during the evaluation. LV and MD provided consultation, helped designing the experiment, and evaluated the results. MD initiated the associated research project and was thus involved in the funding acquisition. All co-authors reviewed the manuscript.

Data availability. The met mast data of FINO3 are publicly available from BSH and met mast and lidar data of IJmuiden can be obtained from TNO. The used model data can be made available upon request.

Competing interests. The authors declare that they have no conflict of interest.

Acknowledgements. This research has been supported by the “NEMO – New methods for turbulence measurements and models in offshore wind” project within the Fraunhofer-Gesellschaft ICON programme. Moreover, it was also supported by France Énergies Marines and the French government, managed by the Agence Nationale de la Recherche under the Investissements d’Avenir program, with the reference no. ANR-10- IEED-0006-34 ("DRACCAR-NEMO project"). The WRF simulations were performed on the HPC Cluster MOUSE, located at the University of Oldenburg (Germany), funded by the Federal Ministry for Economic Affairs and Energy (grant no. 03EE3067). We would like to thank the Federal Maritime and Hydrographic Agency (BSH) for providing the met mast data of FINO3, and TNO providing the met mast and lidar data of IJmuiden.

https://doi.org/10.5194/wes-2026-103
Preprint. Discussion started: 18 September 2026

References

Albers, A., Jakobi, T., Rohden, R., and Stoltenjohannes, J.: Influence of Meteorological Variables on Measured Wind Turbine Power Curves, pp. 525–546, The European Wind Energy Conf. & Exhibition, 2007.

Archer, C. L., Colle, B. A., Veron, D. L., Veron, F., and Sienkiewicz, M. J.: On the predominance of unstable atmospheric conditions in the marine boundary layer offshore of the U.S. northeastern coast, Journal of Geophysical Research: Atmospheres, 121, 8869–8885, https://doi.org/10.1002/2016JD024896, 2016.

Banks, R. F., Tiana-Alsina, J., Baldasano, J. M., Rocadenbosch, F., Papayannis, A., Solomos, S., and Tzanis, C. G.: Sensitivity of boundary-layer variables to PBL schemes in the WRF model based on surface meteorological observations, lidar, and radiosondes during the HygrA-CD campaign, Atmospheric Research, 176-177, 185–201, https://doi.org/10.1016/j.atmosres.2016.02.024, 2016.

Bardal, L. M. and Sætran, L. R.: Influence of turbulence intensity on wind turbine power curves, Energy Procedia, 137, 553–558, https://doi.org/10.1016/j.egypro.2017.10.384, 14th Deep Sea Offshore Wind R&D Conference, EERA DeepWind'2017, 2017.

Bazile, E., Le Moigne, P., Van Hyfte, S., Selly, Y., Verrelle, A., Willemet, J.-M., Blanc, P., Monteiro, D., , and Rousset, F.: Preliminary evaluation of the ARRA re-analysis over France : focus on extreme precipitation, EMS Annual Meeting 2025, EMS2025-648, https://doi.org/doi.org/10.5194/ems2025-648, 2025.

Bloom, S. C., Takacs, L. L., Da Silva, A. M., and Ledvina, D.: Data Assimilation Using Incremental Analysis Update, Monthly Weather Review, 124,

Bodini, N., Lundquist, J. K., and Kirincich, A.: Offshore Wind Turbines Will Encounter Very Low Atmospheric Turbulence, Journal of Physics: Conference Series, 1452, 012 023, https://doi.org/10.1088/1742-6596/1452/1/012023, 2020.

Bodini, N., Lundquist, J. K., Livingston, H., and Moriarty, P.: How generalizable is a machine-learning approach for modeling hub-height turbulence intensity?, Journal of Physics: Conference Series, 2265, 022 028, https://doi.org/10.1088/1742-6596/2265/2/022028, 2022.

Bougeault, P. and Lacarrere, P.: Parameterization of Orography-Induced Turbulence in a Mesobeta–Scale Model, Monthly Weather Review, 117, 1872 – 1890, https://doi.org/10.1175/1520-0493(1989)117<1872:POOITI>2.0.CO;2, 1989.

Brousseau, P., Seity, Y., Ricard, D., and Léger, J.: Improvement of the forecast of convective activity from the AROME-France system, Quarterly Journal of the Royal Meteorological Society, 142, 2231–2243, https://doi.org/https://doi.org/10.1002/qj.2822, 2016.

Bundesamt für Seeschifffahrt und Hydrographie: FINO – Datenbankinformationen, https://www.bsh.de/DE/THEMEN/Beobachtungssysteme/Messnetz-MARNET/FINO/fino_node.htm/, 2021.

Clifton, A. and Wagner, R.: Accounting for the effect of turbulence on wind turbine power curves, Journal of Physics: Conference Series, 524, 012 109, https://doi.org/10.1088/1742-6596/524/1/012109, 2014.

Cuxart, J., Bougeault, P., and Redelsperger, J.-L.: A turbulence scheme allowing for mesoscale and large-eddy simulations, Quarterly Journal of the Royal Meteorological Society, 126, 1–30, https://doi.org/https://doi.org/10.1002/qj.49712656202, 2000.

Deppe, A. J., Gallus, W. A., and Takle, E. S.: A WRF ensemble for improved wind speed forecasts at turbine height, Wea. Forecasting, 28, 212–228, https://doi.org/https://doi.org/10.1175/WAF-D-11-00112.1, 2013.

Dörenkämper, M., Optis, M., Monahan, A., and Steinfeld, G.: On the Offshore advection of Boundary-Layer Structures and the Influence on Offshore Wind Conditions, Boundary-Layer Meteorol., 155, 459–482, https://doi.org/10.1007/s10546-015-0008-x, 2015.

Dörenkämper, M., Olsen, B. T., Witha, B., Hahmann, A. N., Davis, N. N., Barcons, J., Ezber, Y., García-Bustamante, E., González-Rouco, J. F., Navarro, J., Sastre-Marugán, M., Sīle, T., Trei, W., Žagar, M., Badger, J., Gottschall, J., Sanz Rodrigo, J., and Mann, J.: The Making

https://doi.org/10.5194/wes-2026-103
Preprint. Discussion started: 18 September 2026

WIND ENERGY SCIENCE DISCUSSIONS

of the New European Wind Atlas – Part 2: Production and Evaluation, Geosci. Model Dev., 13, 5079–5102, https://doi.org/10.5194/gmd-13-5079-2020, 2020.

Dörenkämper, M., Tambke, J., Steinfeld, G., Heinemann, D., and Kühn, M.: Atmospheric Impacts on Power Curves of Multi-Megawatt Offshore Wind Turbines, J. Phys.: Conf. Ser., 555, 0122 029, https://doi.org/10.1088/1742-6596/555/1/012029, 2014.

Fischereit, J., Brown, R., Larsén, X., Badger, J., and Hawkes, G.: Review of Mesoscale Wind-Farm Parametrizations and Their Applications, Boundary-Layer Meteorology, 182, https://doi.org/10.1007/s10546-021-00652-y, 2022.

Fitch, A. C., Olson, J. B., Lundquist, J. K., Dudhia, J., Gupta, A. K., Michalakes, J., and Barstad, I.: Local and Mesoscale Impacts of Wind Farms as Parameterized in a Mesoscale NWP Model, Monthly Weather Review, 140, 3017 – 3038, https://doi.org/10.1175/MWR-D-11-00352.1, 2012.

Floors, R., Vincent, C., Gryning, S., Peña, A., and Batchvarova, E.: The Wind Profile in the Coastal Boundary Layer: Wind Lidar Measurements and Numerical Modelling, Boundary-Layer Meteorology, 147, 469–491, https://doi.org/10.1007/s10546-012-9791-9, 2013.

Fouquart, Y. and Bonnel, B.: Computations of solar heating of the earth's atmosphere: A new parameterization, Beitr. Phys. Atmos., 53, 35–62, 1980.

Gottschall, J. and Dörenkämper, M.: Understanding and mitigating the impact of data gaps on offshore wind resource estimates, Wind Energy Science, 6, 505–520, https://doi.org/10.5194/wes-6-505-2021, 2021.

Gottschall, J., Catalano, E., Dörenkämper, M., and Witha, B.: The NEWA Ferry Lidar Experiment: Measuring Mesoscale Winds in the Southern Baltic Sea, Remote Sensing, 10, https://doi.org/10.3390/rs10101620, 2018.

Hahmann, A. N., Sīle, T., Witha, B., Davis, N. N., Dörenkämper, M., Ezber, Y., García-Bustamante, E., González-Rouco, J. F., Navarro, J., Olsen, B. T., and Söderberg, S.: The making of the New European Wind Atlas – Part 1: Model sensitivity, Geosci. Model Dev., 13, 5053–5078, https://doi.org/10.5194/gmd-13-5053-2020, 2020.

Hersbach, H., Bell, B., Berrisford, P., Hirahara, S., Horányi, A., Muñoz-Sabater, J., Nicolas, J., Peubey, C., Radu, R., Schepers, D., and et al.: The ERA5 global reanalysis, Quarterly Journal of the Royal Meteorological Society, p. qj.3803, https://doi.org/10.1002/qj.3803, 2020.

Hong, S.-Y., Dudhia, J., and Chen, S.-H.: A Revised Approach to Ice Microphysical Processes for the Bulk Parameterization of Clouds and Precipitation, Monthly Weather Review, 132, 103 – 120, https://doi.org/10.1175/1520-0493(2004)132<0103:ARATIM>2.0.CO;2, 2004.

Hong, S.-Y., Noh, Y., and Dudhia, J.: A New Vertical Diffusion Package with an Explicit Treatment of Entrainment Processes, Monthly Weather Review, 134, 2318 – 2341, https://doi.org/10.1175/MWR3199.1, 2006.

Iacono, M. J., Delamere, J. S., Mlawer, E. J., Shephard, M. W., Clough, S. A., and Collins, W. D.: Radiative forcing by long-lived greenhouse gases: Calculations with the AER radiative transfer models, Journal of Geophysical Research: Atmospheres, 113, https://doi.org/https://doi.org/10.1029/2008JD009944, 2008.

Jiménez, P. A., Dudhia, J., González-Rouco, J. F., Navarro, J., Montávez, J. P., and García-Bustamante, E.: A Revised Scheme for the WRF Surface Layer Formulation, Monthly Weather Review, 140, 898 – 918, https://doi.org/10.1175/MWR-D-11-00056.1, 2012.

Jourdier, B.: Evaluation of ERA5, MERRA-2, COSMO-REA6, NEWA and AROME to simulate wind power production over France, Advances in Science and Research, 17, 63–77, https://doi.org/10.5194/asr-17-63-2020, 2020.

Kaiser, K., Langreder, W., Hohlen, H., and Højstrup, J.: Turbulence Correction for Power Curves, pp. 159–162, Wind Energy, https://doi.org/10.1007/978-3-540-33866-6_28, 2007.

Khanjari, A., Feroz, A., and Archer, C. L.: An analytical formulation for turbulence kinetic energy added by wind turbines based on large-eddy simulation, Wind Energy Science, 10, 887–905, https://doi.org/10.5194/wes-10-887-2025, 2025.

https://doi.org/10.5194/wes-2026-103
Preprint. Discussion started: 18 September 2026

Kilroy, G., Englberger, A., Wrba, L., Bührend, L., and Wildmann, N.: Evaluation of turbulence characteristics in WRF simulations at WiValdi wind park, Journal of Physics: Conference Series, 2767, 052 063, https://doi.org/10.1088/1742-6596/2767/5/052063, 2024.

Larsén, X.: Calculating Turbulence Intensity from mesoscale modeled Turbulence Kinetic Energy, no. E-0233 in DTU Wind Energy E, DTU Wind and Energy Systems, 2022.

Larsén, X. G., Imberger, M., and Floors, R.: Modelling global offshore turbulence intensity including large-scale turbulence, stability and sea state, Wind Energy Science Discussions, 2025, https://doi.org/10.5194/wes-2025-245, 2025.

Lundquist, J. and Clifton, A.: How turbulence can impact power performance, North American Windpower, 9, 13–18, 2012.

Masson, V., Le Moigne, P., Martin, E., Faroux, S., Alias, A., Alkama, R., Belamari, S., Barbu, A., Boone, A., Bouyssel, F., Brousseau, P., Brun, E., Calvet, J.-C., Carrer, D., Decharme, B., Delire, C., Donier, S., Essaouini, K., Gibelin, A.-L., Giordani, H., Habets, F., Jidane, M., Kerdraon, G., Kourzeneva, E., Lafaysse, M., Lafont, S., Lebeaupin Brossier, C., Lemonsu, A., Mahfouf, J.-F., Marguinaud, P., Mokhtari, M., Morin, S., Pigeon, G., Salgado, R., Seity, Y., Taillefer, F., Tanguy, G., Tulet, P., Vincendon, B., Vionnet, V., and Voldoire, A.: The SURFEXv7.2 land and ocean surface platform for coupled or offline simulation of earth surface variables and fluxes, Geoscientific Model Development, 6, 929–960, https://doi.org/10.5194/gmd-6-929-2013, 2013.

Maureira Poveda, J. and Wouters, D.: Wind Measurements at meteorological Mast Ijmuiden, Tech. Rep. ECN-E–14-058, ECN Wind Energy, 2015.

MEASNET: Evaluation of Site-Specific Wind Conditions: Version 2, 2016.

Mlawer, E. J., Taubman, S. J., Brown, P. D., Iacono, M. J., and Clough, S. A.: Radiative transfer for inhomogeneous atmospheres: RRTM, a validated correlated-k model for the longwave, Journal of Geophysical Research: Atmospheres, 102, 16 663–16 682, https://doi.org/https://doi.org/10.1029/97JD00237, 1997.

Nakanishi, M. and Niino, H.: An Improved Mellor Yamada Level-3 Model: Its Numerical Stability and Application to a Regional Prediction of Advection Fog, Boundary-Layer Meteorology, 119, 397–407, https://doi.org/10.1007/s10546-005-9030-8, 2006.

Nakanishi, M. and Niino, H.: Development of an Improved Turbulence Closure Model for the Atmospheric Boundary Layer, Journal of the Meteorological Society of Japan. Ser. II, 87, 895–912, https://doi.org/10.2151/jmsj.87.895, 2009.

Newman, J. F., Klein, P. M., Wharton, S., Sathe, A., Bonin, T. A., Chilson, P. B., and Muschinski, A.: Evaluation of three lidar scanning strategies for turbulence measurements, Atmospheric Measurement Techniques, 9, 1993–2013, https://doi.org/10.5194/amt-9-1993-2016, 2016.

Olson, J. B., Kenyon, J. S., Angevine, W. A., Brown, J. M., Pagowski, M., and Sušelj, K.: A Description of the MYNN-EDMF Scheme and the Coupling to Other Components in WRF–ARW, NOAA Technical Memorandum, https://doi.org/https://doi.org/10.25923/N9WM-BE49, 2019.

Pergaud, J., Masson, V., Malardel, S., and Couvreux, F.: A Parameterization of Dry Thermals and Shallow Cumuli for Mesoscale Numerical Weather Prediction, Boundary-Layer Meteorology, 132, 83–106, https://doi.org/10.1007/s10546-009-9388-0, 2009.

Peña, A. and Mirocha, J. D.: One-year-long turbulence measurements and modeling using large-eddy simulation domains in the Weather Research and Forecasting model, Applied Energy, 363, 123 069, https://doi.org/10.1016/j.apenergy.2024.123069, 2024.

Peña, A. and Santos, P.: Lidar Observations and Numerical Simulations of an Atmospheric Hydraulic Jump and Mountain Waves, Journal of Geophysical Research: Atmospheres, 126, e2020JD033 744, https://doi.org/https://doi.org/10.1029/2020JD033744, 2021.

Pinty, J.-P. and Jabouille, P.: A mixed-phase cloud parameterization for use in a mesoscale non-hydrostatic model: Simulations of a squall line and of orographic precipitation, pp. 217–220, In Proceedings of the AMS conference on cloud physics, 1998.

Ren, G., Liu, J., Wan, J., Li, F., Guo, Y., and Yu, D.: The analysis of turbulence intensity based on wind speed data in onshore wind farms, Renewable Energy, 123, 756–766, https://doi.org/10.1016/j.renene.2018.02.080, 2018.

Ridal, M., Bazile, E., Le Moigne, P., Randriamampianina, R., Schimanke, S., Andrae, U., Berggren, L., Brousseau, P., Dahlgren, P., Edvinsson, L., El-Said, A., Glinton, M., Hagelin, S., Hopsch, S., Isaksson, L., Medeiros, P., Olsson, E., Unden, P., and Wang, Z. Q.: CERRA, the Copernicus European Regional Reanalysis system, Quarterly Journal of the Royal Meteorological Society, 150, 3385–3411, https://doi.org/https://doi.org/10.1002/qj.4764, 2024.

Robey, R. and Lundquist, J. K.: Behavior and mechanisms of Doppler wind lidar error in varying stability regimes, Atmospheric Measurement Techniques, 15, 4585–4622, https://doi.org/10.5194/amt-15-4585-2022, 2022.

Rohrig, K., Berkhout, V., Callies, D., Durstewitz, M., Faulstich, S., Hahn, B., Jung, M., Pauscher, L., Seibel, A., Shan, M., Siefert, M., Steffen, J., Collmann, M., Czichon, S., Dörenkämper, M., Gottschall, J., Lange, B., Ruhle, A., Sayer, F., Stoevesandt, B., and Wenske, J.: Powering the 21st century by wind energy—Options, facts, figures, Applied Physics Reviews, 6, 031 303, https://doi.org/10.1063/1.5089877, 2019.

Rosen, A. and Sheinman, Y.: The average output power of a wind turbine in a turbulent wind, Journal of Wind Engineering and Industrial Aerodynamics, 51, 287–302, https://doi.org/10.1016/0167-6105(94)90064-7, 1994.

Saadatabadi, A. R., Hamzeh, N. H., Kaskaoutis, D. G., Ghasabi, Z., Penchah, M. M., Sotiropoulou, R.-E. P., and Habibi, M.: Optimization and Evaluation of the Weather Research and Forecasting (WRF) Model for Wind Energy Resource Assessment and Mapping in Iran, Applied Sciences, 14, https://doi.org/10.3390/app14083304, 2024.

Saint-Drenan, Y.-M., Besseau, R., Jansen, M., Staffell, I., Troccoli, A., Dubus, L., Schmidt, J., Gruber, K., Simões, S. G., and Heier, S.: A parametric model for wind turbine power curves incorporating environmental conditions, Renewable Energy, 157, 754–768, https://doi.org/https://doi.org/10.1016/j.renene.2020.04.123, 2020.

Sathe, A. and Mann, J.: A review of turbulence measurements using ground-based wind lidars, Atmospheric Measurement Techniques, 6, 3147–3167, https://doi.org/10.5194/amt-6-3147-2013, 2013.

Sathyanadh, A., Prabha, T. V., Balaji, B., Resmi, E., and Karipot, A.: Evaluation of WRF PBL parameterization schemes against direct observations during a dry event over the Ganges valley, Atmospheric Research, 193, 125–141, https://doi.org/10.1016/j.atmosres.2017.02.016, 2017.

Seity, Y., Brousseau, P., Malardel, S., Hello, G., Bénard, P., Bouttier, F., Lac, C., and Masson, V.: The AROME-France Convective-Scale Operational Model, Monthly Weather Review, 139, 976 – 991, https://doi.org/10.1175/2010MWR3425.1, 2011.

Sheinman, Y. and Rosen, A.: A dynamic model of the influence of turbulence on the power output of a wind turbine, Journal of Wind Engineering and Industrial Aerodynamics, 39, 329–341, https://doi.org/10.1016/0167-6105(92)90557-Q, 1992.

Shin, H. H. and Hong, S.-Y.: Representation of the Subgrid-Scale Turbulent Transport in Convective Boundary Layers at Gray-Zone Resolutions, Monthly Weather Review, 143, 250 – 271, https://doi.org/10.1175/MWR-D-14-00116.1, 2015.

Siddiqui, M. S., Rasheed, A., Kvamsdal, T., and Tabib, M.: Effect of Turbulence Intensity on the Performance of an Offshore Vertical Axis Wind Turbine, Energy Procedia, 80, 312–320, https://doi.org/10.1016/j.egypro.2015.11.435, 12th Deep Sea Offshore Wind R&D Conference, EERA DeepWind'2015, 2015.

Skamarock, W., Klemp, J., Dudhia, J., Gill, D., Liu, Z., Berner, J., Wang, W., Powers, J., Duda, M. G., Barker, D., and Huang, X.-Y.: A description of the advanced research WRF version 4.1, Tech. Rep. NCAR/TN-556+ STR, NCAR - National Center for Atmospheric Research, Boulder, Colorado, USA, 2019.

Stark, J. D., Donlon, C. J., Martin, M. J., and McCulloch, M. E.: OSTIA : An operational, high resolution, real time, global sea surface temperature analysis system, in: OCEANS 2007 - Europe, pp. 1–4, https://doi.org/10.1109/OCEANSE.2007.4302251, 2007.

Tai, S.-L., Berg, L. K., Krishnamurthy, R., Newsom, R., and Kirincich, A.: Validation of turbulence intensity as simulated by the Weather Research and Forecasting model off the US northeast coast, Wind Energy Science, 8, 433–448, https://doi.org/10.5194/wes-8-433-2023, 2023.

Tewari, M. F. C., Wang, W., Dudhia, J., LeMone, M. A., Mitchell, K., Ek, M., Gayno, G., Wegiel, J., and Cuenca, R. H.: Implementation and verification of the unified Noah land-surface model in the WRF model, Bulletin of the American Meteorological Society, pp. 2165–2170, 2004.

Türk, M. and Emeis, S.: The dependence of offshore turbulence intensity on wind speed, Journal of Wind Engineering and Industrial Aerodynamics, 98, 466–471, https://doi.org/https://doi.org/10.1016/j.jweia.2010.02.005, 2010.

Wharton, S. and Lundquist, J. K.: Assessing atmospheric stability and its impacts on rotor-disk wind characteristics at an onshore wind farm, Wind Energy, 15, 525–546, https://doi.org/10.1002/we.483, 2012a.

Wharton, S. and Lundquist, J. K.: Atmospheric stability affects wind turbine power collection, Environmental Research Letters, 7, 014 005, https://doi.org/10.1088/1748-9326/7/1/014005, 2012b.

Yang, B., Qian, Y., Berg, L. K., Ma, P., Wharton, S., Bulaevskaya, V., Yan, H., Hou, Z., and Shaw, W. J.: Sensitivity of Turbine-Height Wind Speeds to Parameters in Planetary Boundary-Layer and Surface-Layer Schemes in the Weather Research and Forecasting Model, Boundary-Layer Meteorology, 162, 117–142, https://doi.org/https://doi.org/10.1007/s10546-016-0185-2, 2017.

Yang, Q., Berg, L., Pekour, M., Fast, J., Newsom, R., Stoelinga, M., and Finley, C.: Evaluation of WRF-Predicted Near-Hub-Height Winds and Ramp Events over a Pacific Northwest Site with Complex Terrain, Journal of Applied Meteorology and Climatology, 52, 1753–1763, https://doi.org/10.1175/JAMC-D-12-0267.1, 2013.

Yu, E., Bai, R., Chen, X., and Shao, L.: Impact of physical parameterizations on wind simulation with WRF V3.9.1.1 under stable conditions at planetary boundary layer gray-zone resolution: a case study over the coastal regions of North China, Geoscientific Model Development, 15, 8111–8134, https://doi.org/10.5194/gmd-15-8111-2022, 2022.

Zhang, X., Bao, J.-W., Chen, B., and Grell, E. D.: A Three-Dimensional Scale-Adaptive Turbulent Kinetic Energy Scheme in the WRF-ARW Model, Monthly Weather Review, 146, 2023 – 2045, https://doi.org/10.1175/MWR-D-17-0356.1, 2018.